Received: 18 August 2020 | Revised: 8 May 2021 | Accepted: 20 June 2021

DOI: 10.1111/bre.12591

RESEARCH ARTICLE

Basin Research | IAS EAGE | WILEY

Delta-to-fan source-to-sink coupling as a fundamental control on the delivery of coarse clastics to deepwater: Insights from stratigraphic forward modelling

Chenglin Gong[1,2] | **Dongwei Li**[2] | **Ronald J. Steel**[3] | **Yang Peng**[2] | **Shaohua Xu**[4] | **Yingmin Wang**[2]

[1]State Key Laboratory of Petroleum Resources and Prospecting, China University of Petroleum (Beijing), Beijing, China

[2]College of Geosciences, China University of Petroleum (Beijing), Beijing, China

[3]Department of Geological Sciences, Jackson School of Geosciences, University of Texas, Austin, TX, USA

[4]Chongqing Key Laboratory of Complex Oil and Gas Field Exploration and Development, Chongqing University of Science and Technology, Chongqing, China

Correspondence
Chenglin Gong, College of Geosciences, China University of Petroleum (Beijing), Beijing 102249, China.
Email: chenglingong@cup.edu.cn

Funding information
Science Foundation of China University of Petroleum, Grant/Award Number: 2462020YXZZ020; National Natural Science Foundation of China, Grant/Award Number: 41802117 and 41902114

Abstract

We propose that a more readily studied, secondary source-to-sink (S2S) systems can be formed on direct-fed margins, in which shelf-edge deltas are 'sources' and deep-water fans are terminal depositional 'sinks', with channels working as delivery 'conduits' in between. DionisosFlow stratigraphic-forward model, coupled to seismic and borehole data from middle Miocene Pearl River margin, are used to explore physical and conceptual linkages of delta-to-fan S2S systems, with a focus on the predictability of when and how coarse clastics are delivered from the deltas down to the submarine fans. Middle Miocene Pearl River delta-to-fan S2S coupling was stratigraphically enacted in three main ways: (a) deltas that lack downdip fans: high sea level or low sediment supply caused coarse clastics to be stored mainly on inner to outer shelf areas; (b) deltas that are linked downdip to fans: coarse clastics were funneled to submarine fans through slope channels, via direct delta-to-fan S2S linkages created by delta overreach at shelf break or channels extending back to shelf-margin prodeltas; (c) fans that lack updip, coeval deltas: coarse shelf clastics were carried laterally by longshore or other shelf currents, but eventually captured by canyon heads, and then delivered directly to the basin floor. Moreover, our DionisosFlow stratigraphic-forward models suggest that an oscillation in sea-level behaviour from slowly falling to rapidly falling would result in a within-system tract surface occurring within the falling-stage systems tract. This surface is identified as a significant lower-order unconformity in its proximal reaches and as a correlative conformity distally. Within-system tract surfaces are identified by a change in shelf-edge trajectory regimes from flat to slight falling to moderately falling and in architecture from mixed progradation and degradation to dominant degradation. They are coeval with the onset of the deposition of submarine fans linked updip to deltas or lacking updip deltas, highlighting that sandy deposits can be compartmentalized even within a single systems tract.

KEYWORDS

delta-to-fan S2S coupling, forward stratigraphic model, sequence stratigraphy, source-to-sink system, within-system tract surface

1 | INTRODUCTION

1.1 | Challenges in predicting the accumulation of deep-water sands

Allochthonous delivery of coarse clastics from a shelf into a deep-water sink in either marine or lacustrine basins is important for two reasons. First, it is practically significant, since it fosters the largest sediment accumulations on our planet (i.e. submarine fans), which host approximately 35% of all giant oil field discoveries worldwide (e.g. Carvajal & Steel, 2006; Catuneanu et al., 2009; Fisher et al., 2021; Pellegrini et al., 2020; Posamentier et al., 1992). Second, it is important because it records the dynamic linkages and interactions between fluvial or deltaic processes, marine or lacustrine, and gravity-driven processes in deep-water basins (Dixon et al., 2012; Gong et al., 2016; Paumard et al., 2020; Pellegrini et al., 2020; Peng et al., 2017). After several decades of sequence stratigraphy, there have been four main schools of thought regarding necessary conditions for the delivery of terrestrial sands into deep-water. The first is known as the classic accommodation-driven mechanism that emphasizes the exposure of the continental shelf during the sea-level fall as the principle driver of bringing coarse clastics, especially deltaic sands, across the shelf and into deep-water settings (e.g. Mitchum & Van Wagoner, 1991; Posamentier et al., 1992; Vail et al., 1977), but suffers from being less effective in greenhouse intervals (e.g. Sømme et al., 2009). Such early sequence-stratigraphic concept emphasizes that the relative sea-level fall on or below the shelf edge was likely the key mechanism for slope and basin-floor sand delivery (e.g. Posamentier et al., 1992). The second weights the variability of sediment flux and adds sediment supply-drive as a mechanism that allows the delivery even during rising and high-stand of sea level (obvious for narrow shelves but demonstrated also on 100-km-wide shelves; Carvajal & Steel, 2006; Uroza & Steel, 2008), though this mechanism requires mainly large river supply for bringing coarse clastics into deep-water reaches (see also Covault et al., 2007; Zhang et al., 2017). A third school of thought on deep-water sand delivery adds shelf-edge process modulation to aid or hinder delivery across the shelf edge; this filter emphasizes the positive effect of river- (Dixon et al., 2012; Paumard et al., 2019, 2020), or wave- (Jones et al., 2014; Peng et al., 2017; Uroza & Steel, 2008) regimes at the shelf-margin, and tide-dominated shelf-edge environments (see also Gong et al., 2016). A latest fourth school of thought on deep-water sand delivery emphasizes the cumulative effect of sea-level cycles on sediment transport to deepwater (e.g. Harris et al., 2018, 2020; Zhang et al., 2019). Some experimental results demonstrate a poor relationship between the rate of deep-water sediment delivery and the rate of sea-level change, with the largest delivery rates during periods of low sea level in both icehouse and greenhouse conditions (e.g. Harris et al., 2018, 2020).

Highlights

- A more readily studied delta-to-fan coupling were proposed to explain deep-water sediment delivery.
- Within-system tract surfaces were created by sea-level transition from slowly falling to rapidly falling.
- Within-system tract surfaces denote the onset of submarine fan deposition.
- Sandy deposits can be compartmentalized within falling-stage systems tract.

Irrespective of what brings the delivery system to a shelf-edge position and whether accommodation, supply or shelf-edge process regime is the more influential, it is by no means guaranteed that shelf-edge deltaic sands will automatically pass down to toe-of-slope submarine fans (e.g. Dixon et al., 2012; Fisher et al., 2021; Hawie et al., 2019; Kim et al., 2013) (Figure 1). There remains significant uncertainty and debate regarding the transport, erosion and deposition of when and how terrestrial sands are delivered into deepwater (e.g. Covault et al., 2010; Fisher et al., 2021; Gong et al., 2018; Paumard et al., 2020; Sweet et al., 2020). Therefore, the primary objectives of the present study are to address the research hypothesis: with all model inputs the constant sediment supply but fluctuating sea levels, to what extent do delta-to-fan S2S coupling as discussed below affect the delivery of coarse clastics to deepwater.

1.2 | The concepts of delta-to-fan S2S coupling

The holistic S2S approach to the analysis of basins has arisen as a new generation of research, and has emerged with a broader focus than previous approaches (e.g. Allen, 2008; Martinsen et al., 2010; Matenco et al., 2013; Talling et al., 2015). This approach has long attracted attention from both academia and hydrocarbon industry, and is now widely used to explore not only provenance details, but also when and how the clastic sediment budget brought into the basin is partitioned by volume, by facies and by grain size between different segments of the overall dispersal system. On direct-fed margins (sensu Fisher et al., 2021), shelf-margin deltas actively deliver clastic

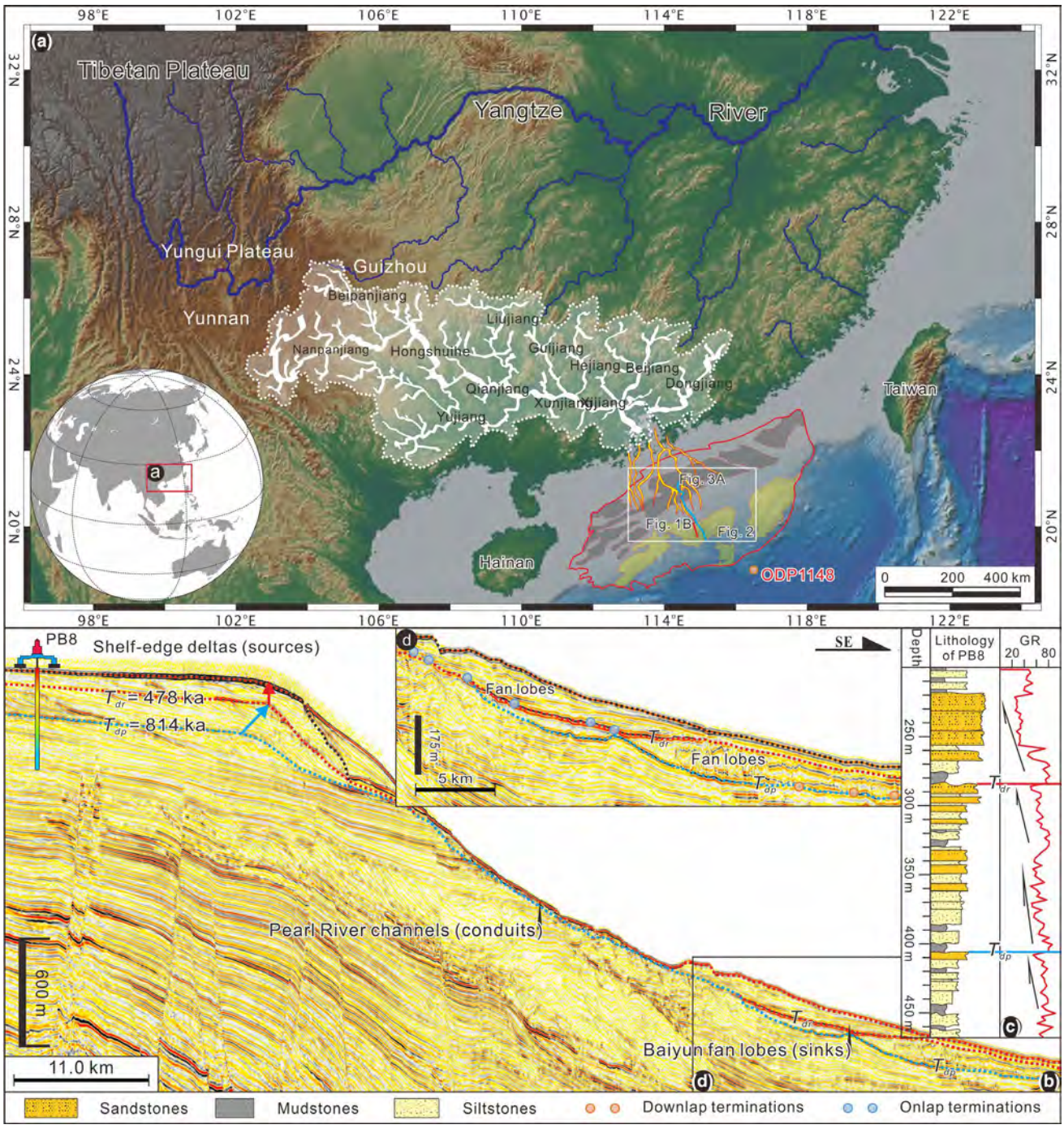

FIGURE 1 (a) Topographic map showing the geographical location and context of the Pearl River S2S systems and map-view locations of seismic lines shown in Figures 1b and 2. Larger study area signifies the domain of DionisosFlow forward numerical modelling (white box). (b–d) Depositional dip-oriented seismic transects and borehole data showing cross-sectional seismic manifestations and lithologies of late Quaternary Pearl River delta-to-fan S2S linkages. T_{dr} and T_{dp} are two basinwide unconformities interpreted to have formed during the middle Pleistocene marine oxygen isotope stage (MIS) 20 (814 ka) and MIS 12 (478 ka) periods of the most pronounced sea-level fall, respectively (see Gong et al., 2018 for full details)

sediments into the deep-water sites to form fans, especially during periods of river flooding or sea-level lowstands. We, therefore, propose a more detailed analysis of the linkages involved in the shelf delta-to-fan S2S coupling from the shelf-edge 'sources' to terminal depositional 'sinks' of deep-water fans, with slope channels functioning as intermediate delivery 'conduits' (Figure 1b). From a S2S perspective, terrestrial sands are first transported and

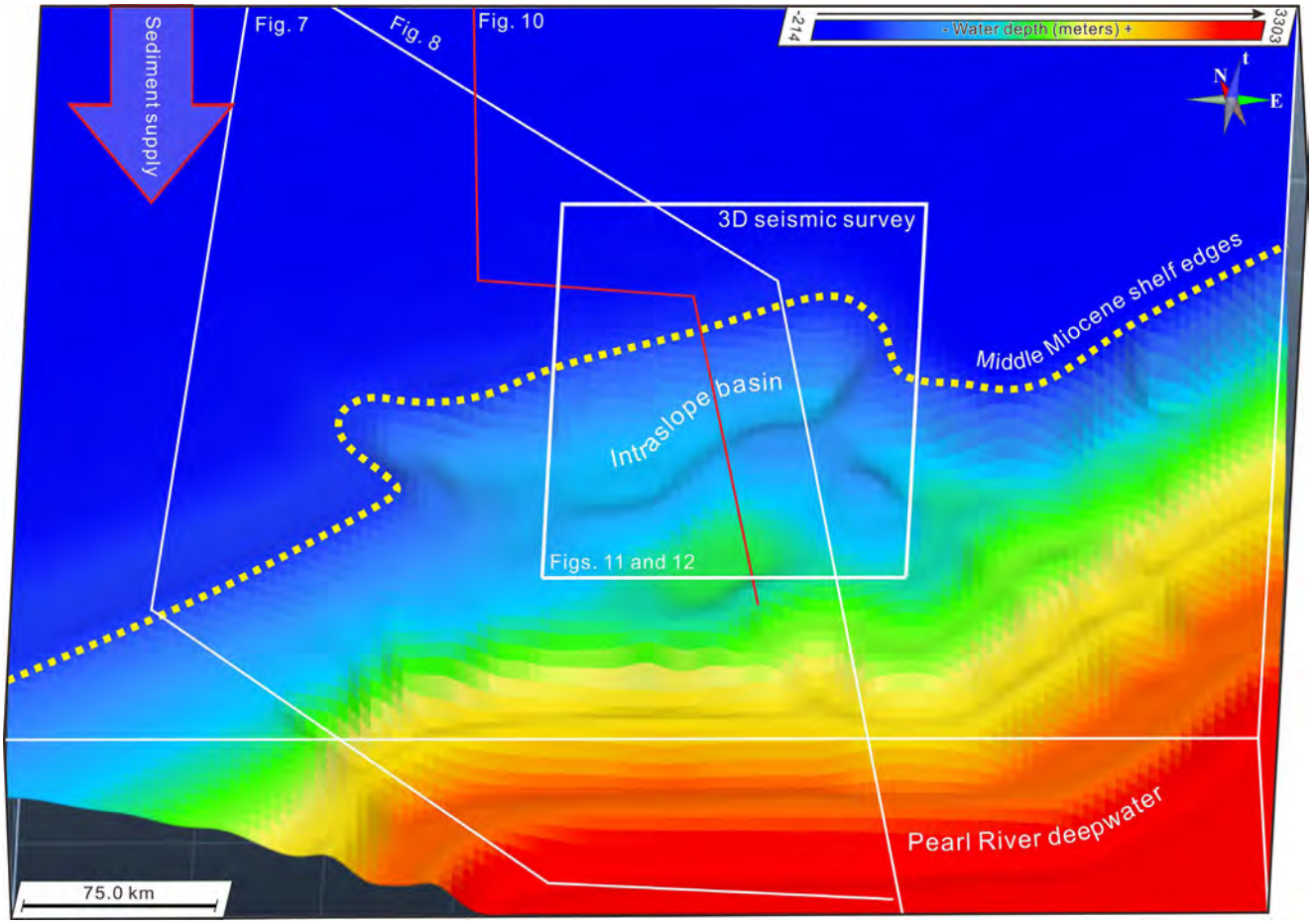

FIGURE 2 Topographic map of the Pearl River margins (i.e. the domain of the DionisosFlow forward numerical model) showing plan-view locations of dip-oriented sections of DionisosFlow forward numerical models shown in Figures 7, 8, and 10. Also shown are map-view locations of the perspective maps of RMS attributes shown in Figures 11 and 12 (i.e. 3D seismic survey of the present study)

deposited from river systems to inner-, middle- and shelf-edge deltas on direct-fed margins (Fisher et al., 2021), some of which disperse sediments further into deep-water areas to form submarine fans (Covault et al., 2010; Fisher et al., 2021; Gong et al., 2018; Paumard et al., 2020). Shelf-to-basin deep-water sand delivery on direct-fed margins is, thus, achieved through the agencies of delta-to-fan S2S coupling that play a significant but underappreciated role in the modulation of deep-water sand delivery and are the focus of the present study.

Using a seismic and borehole database from the submarine segments of middle Miocene Pearl-River shelf-margin systems, coupled to DionisosFlow stratigraphic-forward models, the current research aims to investigate the physical and conceptual coupling of delta to deep-water fan systems with a tie to reservoir prediction. Understanding physical and conceptual linkages between shelf-edge deltas and concomitant deep-water fans is of paramount importance to predict when, how, and where reservoir-quality sands were delivered into deep-water areas.

2 | SUBMARINE SEGMENTS OF THE PEARL RIVER S2S SYSTEMS

2.1 | Late Quaternary Pearl River delta-to-fan S2S coupling

The study area is located in submarine segments of the Pearl River S2S system (Figures 1 and 2). Pear River originates from the Yungui Plateau (i.e. Maxiong Mountains in Yunnan Province), and has eight main tributaries that have a main stem length of 2,214 km, annual runoff of 3×10^{11} m^3, a mean annual water discharge of 9,600 m^3/s, and an annual suspended sediment discharge of 90 Mt (Wei & Wu, 2011) (Figure 1a). The sediment supply of the paleo-Pearl River had a sand-to-mud ratio of 0.35:0.65, which is typical of a fine-grained system (Shao et al., 2008). The submarine segment of late Quaternary Pearl River S2S system is composed mainly of inner- to outer-shelf deltas and resultant fan lobes on the deepwater slopes and base-of-slope region (Figure 1). Late Quaternary Pearl River

shelf-edge deltas are seismically imaged as delta-scale (<100 m) clinothems with sigmoid-oblique reflection patterns (see Gong et al., 2018 for a detailed seismic interpretation) (Figure 1b), and are characterized by stacked units of coarsening- and thickening-upward facies (Figure 1c). Late Quaternary Pearl River intraslope fan lobes are seismically imaged as wedges with basinward, downlap terminations, and with slopeward, onlap terminations in an upslope direction (Figure 1d). Strongly progradational and strongly aggradational shelf-edge deltas are, respectively, mappably linked downdip to progradational and retrogradational fan lobes in outlying Pearl River deep-water areas (see also Gong et al., 2018 for more details) (Figure 1b–d). In this case, basinward or landward migration of the submarine fans mirrors the migratory behaviour of the upslope coeval shelf-margin deltas, forming a tight coupling between Pearl River shelf-margin deltas and deep-water fans. This example has some similarity to coupling between Washakie Basin shelf-edge deltas and toe-of-slope fans described by Koo et al. (2016).

2.2 | Middle Miocene Pearl River delta-to-fan S2S coupling

As evidenced by the renewal of Antarctic ice sheets, the middle Miocene witnessed a change in global climates from a warmer to a colder stage (e.g. Holbourn et al., 2014). Accordingly, the middle Miocene submarine segment of Pearl River S2S systems witnessed a big sea-level fall (Cao et al., 2018; Lin, He, et al., 2018; Lin, Jiang, et al., 2018; Zhang et al., 2019), resulting in seismically well-imaged

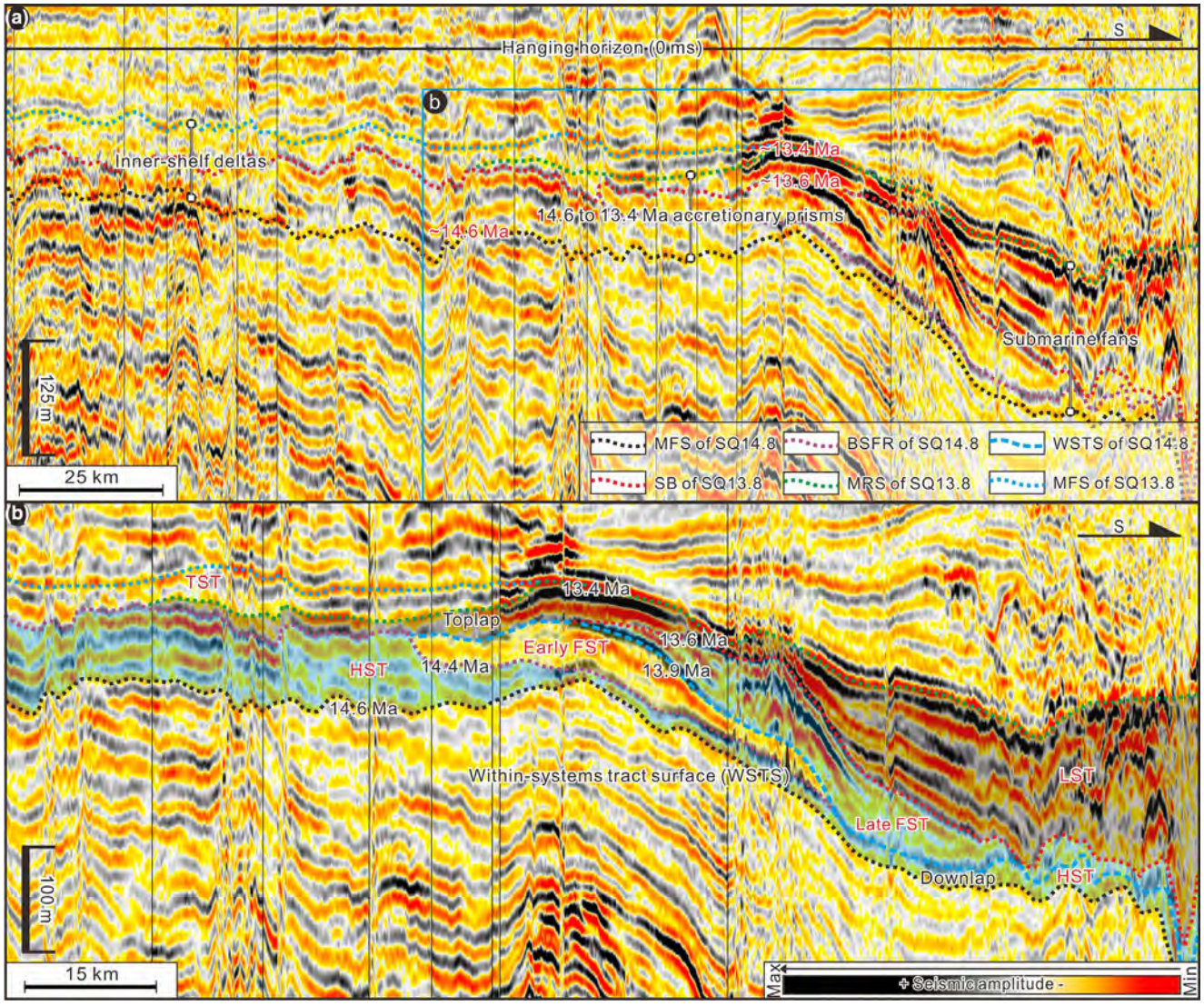

FIGURE 3 (a) Regional seismic line (see line location in Figure 2) across the entire Pearl River margin from the inner shelf down to deepwater showing seismic appearance of middle Miocene Pearl River inner-shelf to shelf-margin deltas and associated deep-water fans. (b) A close-up view of seismically well-imaged middle Miocene Pearl River delta-to-fan systems

delta-to-fan depositional systems (Figure 3a,b). The study interval of interest is bounded at its base by the maximum flooding surface (MFS) of SQ14.8 (dated at 14.6 Ma) and at its top by the MFS of SQ13.8 (dated at 13.4 Ma), with a duration of 1.2 My (Ran et al., 2013; Xie et al., 2009; Xu et al., 2020) (Figure 3a,b). The extracted interval contains shelf-edge deltas seismically imaged as clinothems (height of 10s m) with sigmoid-oblique reflection patterns in the shelf-margin reaches of the system and deep-water fans seismically appeared as prograding and downlapping packages at outlying deep-water reaches, forming a linked delta-to-fan system (Figure 3b). The role and character of this delta-to-fan S2S linkages (height of 100s of m) in determining when, how, and where reservoir-quality sands were delivered and transported from shelf-edge deltas coming down to the Pearl River deepwater region are the focus of the present study.

3 | DATASETS AND METHODOLOGY

3.1 | DionisosFlow forward stratigraphic model

DionisosFlow software is a 4-D process-based deterministic multi-lithology forward stratigraphic model that simulates the first-order evolution of depositional systems at the spatial scale of 10^2–10^3 m and temporal resolution of 10^3–10^5 yr (e.g. Granjeon, 2014; Hawie et al., 2019). For each time step, DionisosFlow is able to numerically calculate three main physical processes, namely the creation of accommodation space (i.e. eustasy, subsidence and compaction), sediment supply (i.e. sediment discharge and water discharge), and the processes of erosion, transport, and deposition of sediment (e.g. Deville et al., 2015; Granjeon, 2014; Zhang, Lin, et al., 2019). DionisosFlow 3D stratigraphic forward model is widely used to explore the interplay of geological factors related to the volume and architecture of depositional systems (e.g. tectonism, sea level, water and sediment supply) (Harris et al., 2016, 2018, 2020; Hawie et al., 2018, 2019). It has been employed herein to explore physical and conceptual linkages of delta to deep-water fan systems and their role in the modulation of deep-water sand delivery beyond the shelf edge.

3.2 | 3D seismic data and boreholes

The primary datasets utilized in the present study include approximately 12,000 km^2 of 3D seismic data (red box in Figure 1a), tied to 21 boreholes. 3D seismic data were acquired and provided by the China National Offshore Oil Corporation, and have been processed using the pre-stack hybrid migration algorithm. They have a sampling interval of 4 ms, and are displayed using SEG negative standard polarity, where a positive reflection coefficient is represented by a positive (peak) reflection event and corresponds to an increase in the acoustic impedance. 3D seismic data have the frequency of 40–50 Hz, giving rise to an estimated vertical resolution of 10–15 m.

This research integrates 'classical' 2D seismic stratigraphy with 3D seismic geomorphology approach, through which seismic stratigraphy and geomorphology of middle Miocene Pearl River delta-to-fan systems are quantitatively analysed and visualized. Root-mean-squares (RMS) amplitudes, which calculate the square root of the sum of the time-domain energy, offer the enhanced visualization of the stratigraphic architecture of small-scale depositional elements. They are, therefore, employed to visually delineate geomorphology and architectures of middle Miocene Pearl River delta-to-fan systems.

4 | FORWARD STRATIGRAPHIC MODEL SETUP

4.1 | Setup of the model domain

4.1.1 | Initial bathymetry and tectonics

We use the seafloor topographic map obtained from the 3D seismic volume as the initial bathymetry (white box in Figure 1a). Past eustatic values in our model are reported with respect to the initial shelf-edge break of the basal bounding surface of the modelled delta-to-fan systems (i.e. the MFS of SQ13.8 seen on seismic lines shown in Figure 3) in the past (i.e. 200 m isobath). The initial bathymetry of our 3D stratigraphic forward model is similar to that of typical passive margins, with water depth of up to 3,000 m, an average value of shelf gradient equal to 0.05°, and an average slope gradient equal to 1.05° (Table 1).

The study area of the Pearl River Mouth Basin evolved into a passive continental margin since the Late Oligocene, with two periods of seafloor expansion. There was a transition from a seafloor-spreading to a post-spreading stage after the late Miocene (Li et al., 2015; Lin, He, et al., 2018; Lin, Jiang, et al., 2018). Lin, Jiang, et al. (2018) have suggested that the mean tectonic subsidence rate decreased to a lower rate of 40 m/Myr from 14.6 to 13.4 Ma, reflecting the post-spreading setting. Consistent with this conclusion, our Pearl River stratigraphic forward model implemented a simple, hinge-style tectonic subsidence with a rate of 0 m/Myr at the most proximal position (i.e. inner shelf) and a rate of up to 200 m/Myr at the most distal position (i.e. deep-water sites).

TABLE 1 A summary of input parameters and associated values and references used for Pearl River DionisosFlow modelling experiments

Domain definition		
Model dimensions (km^2)	189,728	N/A
Average shelf gradient (degree)	0.05°	N/A
Average slope gradient (degree)	1.05°	N/A
X-axis length (m)	484,000	N/A
Y-axis length (m)	392,000	N/A
Grid point spacing (km)	4 (d*x*) × 4 (d*y*)	N/A
Cell number (d*x* × d*y*)	121 × 98	N/A
Scanning radius (m)	5,000	N/A
Bathymetric definition of deepwater (m)	≥200	N/A
Sediment classes and properties		
Mud (% of total sediment load)	75%	Shao et al. (2008)
Sand (% of total sediment load)	25%	Shao et al. (2008)
Sediment classes and properties (mm)	10% sand (0.2)	N/A
	75% shale (0.01)	N/A
	15% silt (0.04)	N/A
Structural evolution		
Tectonic subsidence rate (m/Myr)	0–200	Lin, Jiang, et al. (2018)
Initial substratum thickness	20 m of mudstone	N/A
Eustasy varations		
Sea-level curve (m)	Figure 4	Xu et al. (1995)
Ocean propertes		
Ocean temperature (°C)	20	N/A
Ocean salinity (g/L)	35	N/A
Sediment supply		
Sediment supply (km^3/Myr)	7,000	Wei and Wu (2011)
Water discharge (m^3/s)	7,000	Wei and Wu (2011)
Width of supply point (km)	80	N/A
Position of sediment supply (d*x*)	88,500	N/A
Number of supply point	1	N/A
Suspended sediment concentration of Pearl River (kg/m^3)	0.13–0.34	Wei and Wu (2011)
Suspended sediment concentration of our model (kg/m^3)	0.063	N/A
Wave impact		
Wave base (m)	14.00	N/A
Wave progagation azimuth (°)	60	N/A
Wave frequency in a year	1	N/A
Wave energy flux (kW/m)	95.8	N/A
Wind speed (cm/s)	1,371.0	N/A
Wave period (s)	5.67	N/A
Wave height (m)	5.02	N/A
Transport processes		
Diffusion transport law		
Water-driven transportation (*n*)	1.5	Prosser and Rustomji (2000)
Slope-driven transportation (m)	1.0	
Randomness ratio	0.3	N/A
Low-energy long-term transport model		
Average shelf gradient (m/km)	0.8	N/A
Average slope gradient (m/km)	18.0	N/A
Ration between gravity and water processes	5.0	N/A
High-energy short-term transport model		
HEST/LELT water discharg ration	10	N/A
Relative Duration of the HEST Period (month)	3	N/A
Proportion of sediment flow coming during HEST time	0	N/A
Erosion model		
Basement rate/seidment rate	1	N/A
Maximum weathering decay in marine enviroments	20	Harris et al. (2016, 2020)
Simulation parameters		
Run period of Pearl River model (Ma)	14.6–13.4	N/A
Duration (Myr)	1.2	N/A
Time steps (Myr)	0.03	N/A
Runs of numerical models	40	N/A

(Continues)

4.1.2 | Domain definition (cell sizes and time steps)

Our DionisosFlow model simulation is representing the submarine segments of Pearl River S2S systems, covering an area of 484 × 392 km = 189,728 km^2 (white box in Figure 2) and a run period of 14.6–13.4 Ma (1.2 My) (Figure 3; Table 1). Considering the computing capability of our workstation, we employed a grid point spacing of 4 km (*x*-axis) × 4 km (*y*-axis) and an initial simulated time step of 0.003 Myr, thereby resulting in 11,858 cells and 40 runs of DionisosFlow modelling experiments (Table 1). A domain of this size (11,858 cells and 40 runs of modelling experiments) allowed the model to be computationally efficient. Our individual cell sizes (i.e. 4 × 4 km) are comparable to those of Deville et al. (2015) who used a grid spacing of 10 km (*x*-axis) × 10 km (*y*-axis) to simulate large-scale sediment fairways and facies distribution of Orinoco delta-to-fan systems with an area of 1,200 km × 1,200 km = 1,440,000 km^2.

4.2 | Model input parameters

4.2.1 | Sediment-transport parameters

The aim of the Dionisos is to simulate the first-order evolution of large-scale depositional systems (Harris et al., 2016, 2018, 2020; Hawie et al., 2018, 2019). Sediment transport in DionisosFlow is determined by a nonlinear slope- and water-driven diffusion model (Granjeon, 2014), expressed as follows:

$$Q_s = -\left(K_s/\vec{\nabla}\, h + K_w Q_w^m S^n\right).$$

where Q_s is the sediment discharge (km^3/Myr); K_s and K_w are, respectively, the gravity- and water-driven diffusion coefficients (km^2/kyr); Q_w is the water discharge (m^3/s); n and m are exponents that affect sediment transport capacity related to slope- and water-driven transport, with values ranging from 1 to 2 (Tucker & Slingerland, 1994); h is the topographic elevation (m); $\vec{\nabla}\, h$ is the local topographic gradient or slope (dimensionless) (Harris et al., 2020); and S is the dimensionless gradient of the basin (Granjeon, 2014). All of these sediment-transport input values are listed in Table 1, and were also utilized in many other DionisosFlow forward stratigraphic experiments (Harris et al., 2016, 2018, 2020; Hawie et al., 2018, 2019).

4.2.2 | Sediment-supply parameters

Constant water- and sediment-discharge values analogous to the modern Pearl River were applied to our Pearl River forward stratigraphic models (Table 1). Constant sediment supply is a fundamental assumption of sequence stratigraphic concepts (Posamentier et al., 1988) and a common assumption of DionisosFlow 3D stratigraphic forward models (see also Harris et al., 2016). We, however, recognize that the sediment discharge to a basin is variable at a wide range of spatiotemporal scales. The primary objectives of the present study are to address the research question: with all model inputs the same and constant sediment-supply parameters, what exactly drives shelf-edge deltaic sands into deep-water basins. All of our stratigraphic forward model runs, therefore, employed constant water and sediment discharge rates of 7,000 km^3/Myr and 7,000 m^3/s; consistent with the notion that seven main tributaries of the Pearl River have a mean water discharge of 9584.3 m^3/s and a yearly sediment discharge of 0.13–0.34 kg/km^3 (averaging 0.25 kg/km^3) (Wei & Wu, 2011) (Table 1). These values of water and sediment discharge rate are typical of a modern moderate-size river (Milliman & Syvitski, 1992). Shao et al. (2008) have suggested that the sediment supply of the paleo-Pearl River had a sand-to-mud ratio of 0.35:0.65. Accordingly, our Pearl River stratigraphic forward model implemented a constant sediment load consisting of 35% sand and 65% mud, with grain-size classes composed of 5% coarse sand (0.5 mm), 10% medium sand (0.3 mm), 20% fine sand (0.1 mm), and 65% silt/clay (0.004 nm) (Shao et al., 2008) (Table 1).

4.2.3 | Sea-level oscillations

Our forward stratigraphic model employs the eustatic curve in the Pearl River Mouth Basin, established by Xu et al. (1995). The model implemented ran a timestep of 0.03 Myr spanning the period from 14.6 to 13.4 Ma, during which there was a transition from a warmer to a colder climate stage (known globally as the middle Miocene climate cooling) (Holbourn et al., 2014). This prominent climatic event contributed to a rapid paleoenvironmental change and resultant large sea-level drops of up to −277 m (i.e. negative and positive signs being suggestive of paleo-sea level below and above the modern sea level) (Figure 4). Eustatic sea level in the Pearl River Mouth Basin from 14.5 to 13.6 Ma was between −277.0 and −69.9 m, with a mean value of −152.3 m and a standard deviation of ±87.1 m (Figure 4).

5 | FORWARD STRATIGRAPHIC MODEL RESULTS

The eustatic curve shown in Figure 4 exhibits four different phases of sea-level fluctuation, each of which was taken as the input variable to DionisosFlow forward stratigraphic models (Table 2), and produced a specific delta-to-fan S2S linkage as discussed below.

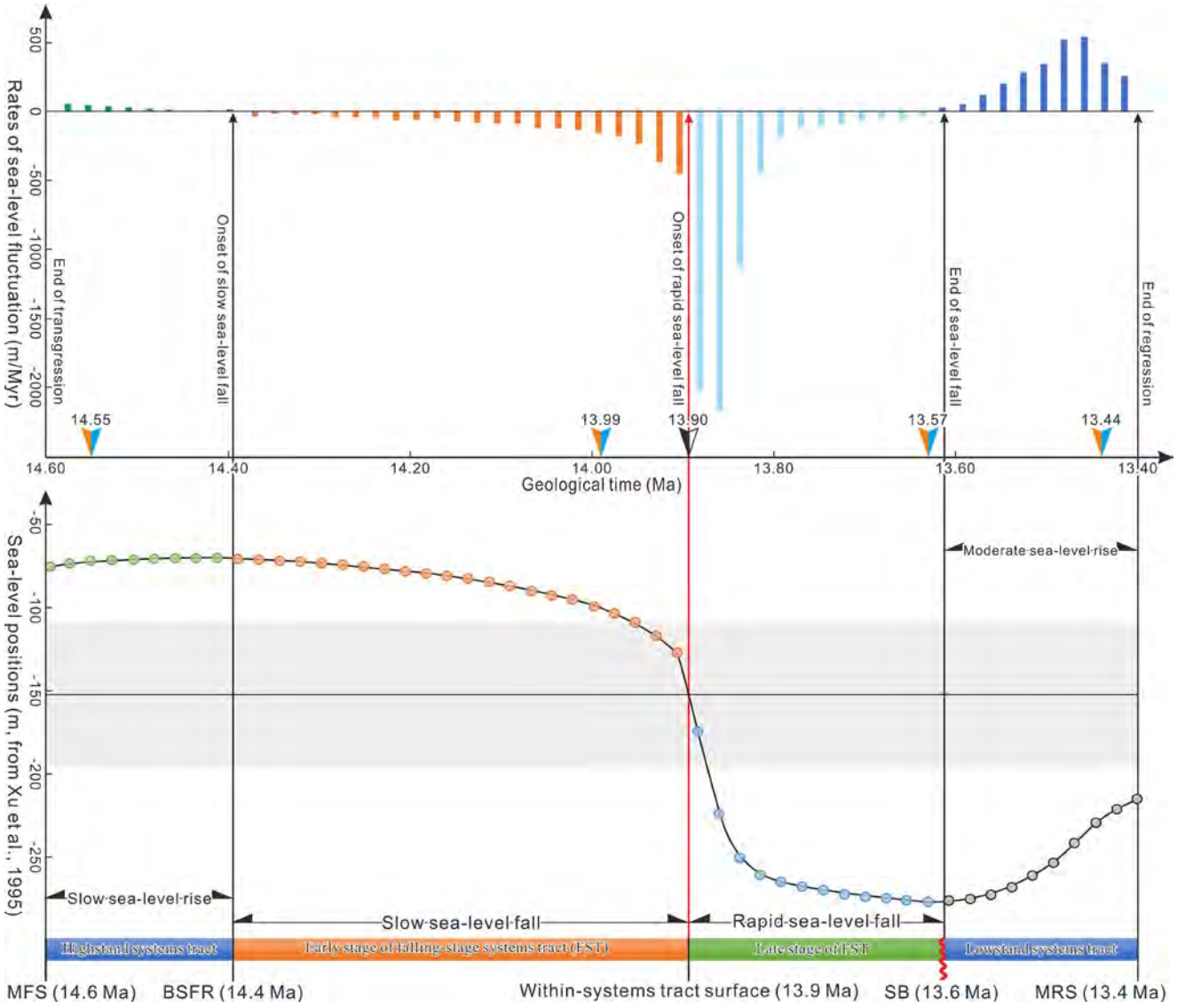

FIGURE 4 Eustatic sea-level fluctuation from 14.6 to 13.4 Ma, as calculated from the eustatic database of Xu et al. (1995). Solid line denotes the mean sea-level position of −152.3 m. The solid box outlines the standard deviation of ±87.1 m. The shown eustatic sea-level curve display four main patterns of sea-level fluctuations, each of which corresponds to a specific systems tract

TABLE 2 A summary of sediment concentration of main tributaries of the Pearl River (compiled from Wei & Wu, 2011)

	Water discharge			Suspended load		
Tributary	Annual amount (10^8, m^3)	Mean discharge (m^3/s)	Percentage	Concentration (kg/m^3)	Annual amount (10^4, t)	Percentage
Xijiang	2,220	7,020	73.29	0.32	7,100	80.03
Beijiang	413	1,310	13.63	0.13	647	7.29
Dongjiang	233	737	7.69	0.13	296	3.34
Suijiang	68.4	217	2.26	0.16	109	1.23
Zengjiang	38.2	121	1.26	0.14	56.1	0.63
Liuxihe	18.7	59.4	0.62	0.06	10.2	0.11
Tanjiang	20.7	65.5	0.68	0.11	23.0	0.26
The rest	17.1	N/A	0.56	N/A	630.7	7.11
Total	3,029.1	9,584.3	1	0.13–0.34	8,872	1

5.1 | Slow sea-level rise: Deltas lacking downdip fans

The early stage of eustatic sea-level fluctuation (i.e. 14.600–14.416 Ma) displays low rates of the sea-level rise ranging from 6.51 to 54.67 m/Myr, with a mean value of 25.62 m/Myr and a standard deviation of ±16 m/Myr, showing a sea-level behaviour referred to herein as *slow sea-level rise* (Figure 4). During the slow sea-level rise, sandy deposits (sand percentages of >30%) are seen to disperse on the inner shelf, resulting in inner-shelf delta-front migration (Figures 5a, 7a, and 8a). These inner-shelf deltas are seen as thin, low-angle deltaic clinoforms in cross-sectional view, and lack any severe erosion or cannibalization (Figures 7a and 8a). By definition, the deltas are far from the shelf edge (>100 km), so no sand passes the shelf edge to form any submarine fans.

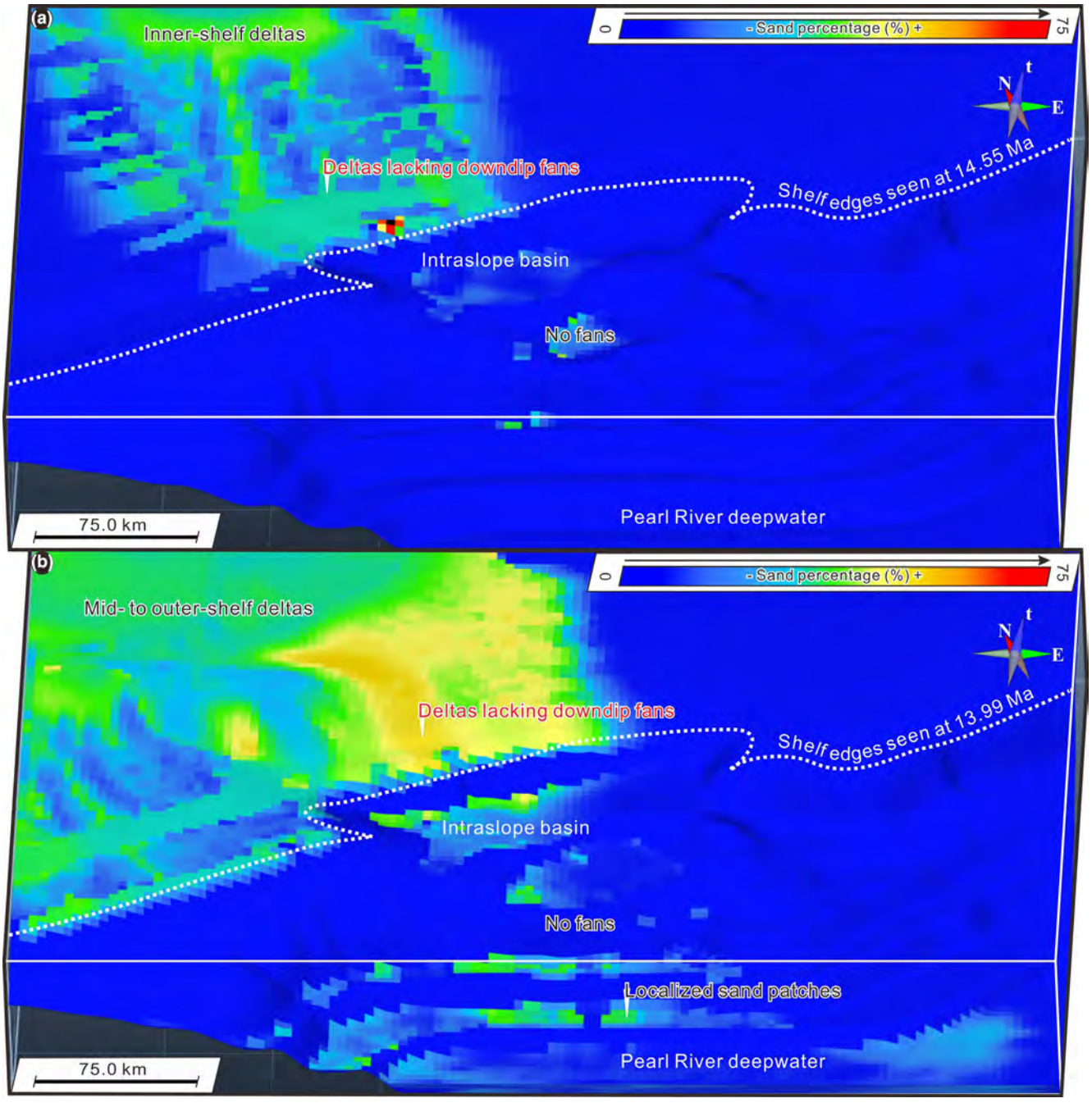

FIGURE 5 Representative snapshots of DionisosFlow forward numerical models of slow sea-level rise and slow sea-level fall (upper and lower panels, respectively). Note that grain-size distribution patterns at 14.55 Ma and 13.99 Ma (upper and lower panels, respectively) illustrating linkages of deltas lacking downdip fans. Please refer to Figures 2 and 4 for plan-view locations and stratigraphic positions of the shown snapshots

5.2 | Slow sea-level fall: Deltas lacking downdip fans

During the early to middle stages of the eustatic sea-level fluctuation run (i.e. 14.41−13.63 Ma age), there were low rates of sea-level fall of −454.12 to −17.11 m/Myr, with a mean value of −113.95 m/Myr and a standard deviation of ±109.20 m/Myr, showing a sea-level behaviour referred to herein as *slow sea-level fall* (Figure 4). Driven by the slow sea-level fall, the sandy deltas with sand percentages of >30% have prograded onto the middle to outer reaches of the Pearl River shelf (Figures 5b and 8b). These mid to outer-shelf deltas are seen as low-angle-dipping deltaic clinoforms (delta height averaging 30 m), with a lack of any severe erosion or cannibalization (Figures 7b and 8b). During this period of the slow sea-level fall, the Pearl River deepwater slope or toe-of-slope received no extensive sand accumulation (Figures 5b, 7b, and 8b). In this scenario, mid- to outer-shelf deltas sporadically reached, but were not able to maintain a shelf-edge position, thereby disfavoring the delivery of coarse clastics into the Pearl River deepwater areas (Figures 5b, 7b and 8b).

5.3 | Rapid sea-level fall: Deltas linked downdip to fans

The late middle stage of the eustatic sea-level fluctuation run (i.e. 13.910–13.634 Ma age) exhibits high rates of sea-level fall ranging from −2,172.61 to −34.59 m/Myr, with a mean value of −541.45 m/Myr and a standard deviation of ±758.83 m/Myr, showing a sea-level behaviour referred to herein as *rapid sea-level fall* (Figure 4). Driven by the rapid sea-level fall, sandy deposits with sand percentages of >30% have prograded onto the Pearl River shelf-margin areas, and maintained a shelf-edge position, forming shelf-margin deltas (Figures 6a and 7c). These shelf-margin deltas draped across the pre-existing shelf edge, and were probably eroded by their own fluvial distributaries with sinuous fairways and U- to V-shaped geometries (i.e. incised channels) (Figures 6a and 7c). Only fragments of them are seen to be preserved on the outer Pearl River shelf (Figures 7c and 8c), indicating significant shelf-edge erosion and cannibalization of shelf-margin deltas (see analogous outcrop example from Mellere et al., 2003). Driven by the rapid sea-level fall, there developed a clear linkage of shelf-edge deltas and some distributary channel belts to deepwater slope channels, resulting in the extensive toe of slope fans with sand percentages of >30% (Figures 6a and 7c). In this scenario, shelf-edge deltas suffered significant fluvial erosion, and as expected formed downdip, time-equivalent submarine fans (Figures 6a and 7c).

5.4 | Moderate sea-level rise: Deltas linked downdip to fans or fans lacking updip deltas

The last stage of the eustatic sea-level fluctuation run (i.e. 13.634–13.400 Ma) displays the modest rates of sea-level rise of 26.59–539.67 m/Myr, with a mean value of 267.58 m/Myr and standard deviation of ±167.32 m/Myr, showing a sea-level behaviour referred to herein as *moderate sea-level rise* (Figure 4). Driven by the moderate sea-level rise and continued sediment supply, the shelf-margin deltas with sand percentages of >30% were able to re-establish after the falling sea-level cannibalization and clearly re-established and maintained a shelf-edge position (Figures 7d and 8d), forming lowstand wedges (sensu Posamentier & Vail, 1988) or lowstand shelf-margin deltas (sensu Steel et al., 2003) (Figures 6b and 7c). These lowstand shelf-margin deltas, nevertheless were still subject to downcutting and erosion by incised channels with sinuous fairways and U- to V-shaped cross-sections, and were able to link downdip to slope channels (Figures 6b and 7d). They lap down onto the slope, with only some fragments being well preserved on the outer Pearl River shelf because of channel incisions (Figures 7d and 8d). Similar to what happened during the rapid sea-level fall, areally extensive toe-of-slope fans are seen to have developed (Figures 6b and 7d). In this scenario, shelf-edge deltas were subject to significant fluvial erosion by shelf valleys characterized by sinuous fairways and U- to V-shaped cross-sections, and as expected formed downdip, time-equivalent submarine fans (Figures 6b and 7d).

In marked contrast to the scenario of the rapid sea-level fall, submarine fans expressed as lobate sand accumulations with sand percentages of >30% are seen to occur in the southeastern corner of our DionisosFlow forward model domain that lack updip, time-equivalent shelf-margin deltas (Figures 6b and 8d), showing a linkage of fans lacking updip deltas. In this scenario, shelf-edge deltas most likely suffered wholesale shelf-edge erosion or collapse or were influenced by wave-dominated processes, creating the downdip, time-equivalent submarine fans (Figures 6a and 7c).

6 | VERIFICATION OF THE FORWARD STRATIGRAPHIC MODEL USING SEISMIC DATA

The results of each of the above four stages of modeled sea-level change can be compared with the corresponding clinothem stacking patterns and delta-to-fan S2S linkages seen in the stratigraphy of the middle Miocene Pearl River margin.

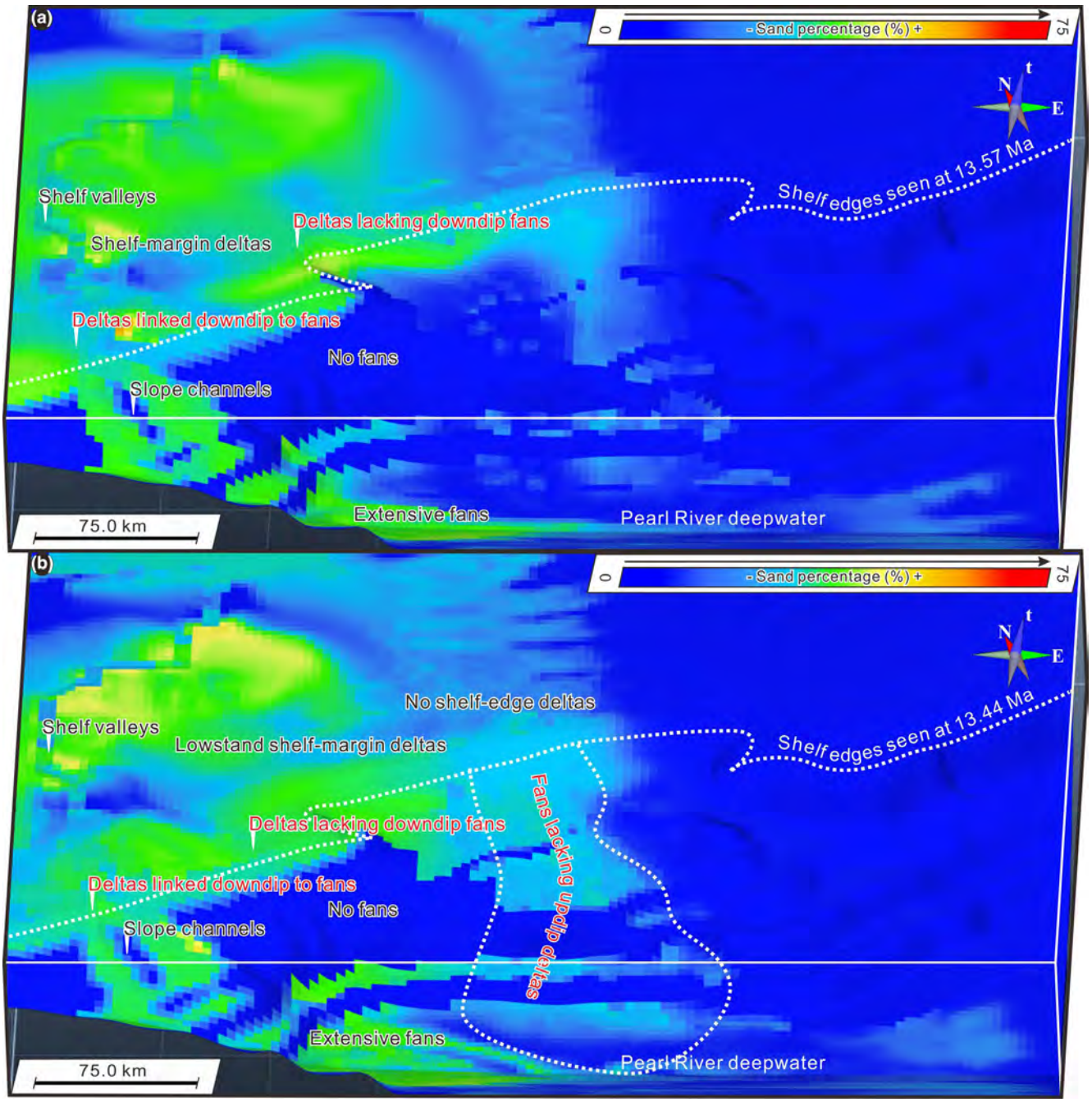

FIGURE 6 Representative snapshots of DionisosFlow forward numerical models of rapid sea-level fall and moderate sea-level rise (upper and lower panels, respectively). Note that grain-size distribution patterns at 13.57 Ma and 13.44 Ma (upper and lower panels, respectively) illustrate three main types of delta-to-fan S2S linkages, including deltas lacking downdip fans, deltas linked downdip to fans, and fans lacking updip deltas. Please refer to Figures 2 and 4 for plan-view location and stratigraphic position of the shown snapshots

6.1 | Pearl River margin highstand system tract: Deltas lack downdip fans

Seismic-well ties verify that the basal bounding surfaces of the interval of slow sea-level rise correspond to the maximum flooding surface of SQ14.8 (i.e. MSF of SQ14.8 dated at 14.6 Ma) (Figures 3, 4, and 9). The upper bounding surfaces of the interval of slow sea-level rise correspond to the basal surface of the forced regression (sensu Hunt & Tucker, 1992) or the subaerial erosional truncation surfaces (sensu Martin et al., 2009) of SQ14.8 (i.e. BSFR of SQ14.8 dated at 14.4 Ma) (Figures 3, 4, and 9). MSF of SQ14.8 and BSFR of SQ14.8, respectively, denote the end of sea-level transgression and the onset of slow sea-level fall (Figure 4). Clinothems on middle Miocene Pearl River margin spanning the above time interval display an overall aggradational to progradational stacking

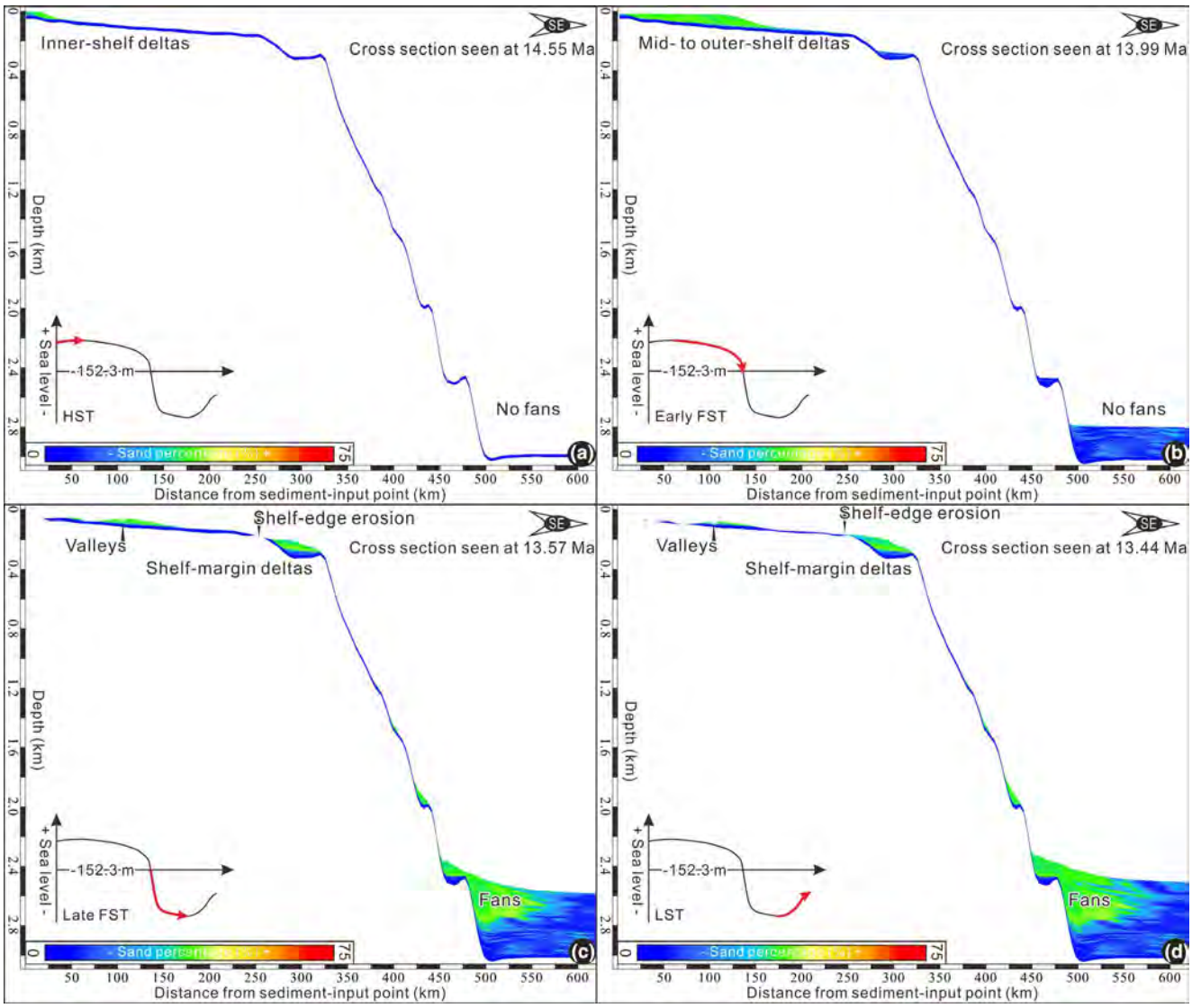

FIGURE 7 Dip-oriented sections of DionisosFlow forward numerical models (see their plan-view and stratigraphic locations in Figures 2 and 4, respectively) illustrating patterns of grain-size distribution at 14.55 Ma (a), 13.90 Ma (b), 13.57 Ma (c) and 13.44 Ma (d). Note that deltas seen in cross sections of panels A and B of this figure lack downdip fans, but that deltas seen in cross sections of panels C and D of this figure are linked downdip to submarine fans

(AP stacking sensu Neal & Abreu, 2009) that is indicative of rates of coastal accommodation creation and sedimentation fill ($\delta A/\delta S$) < 1 and normal regression of the shoreline (Neal & Abreu, 2009) (i.e. highstand system tract) (Figures 3 and 9).

Architecturally, Pearl River HST of 14.6–14.4 Ma age is composed of deltaic progradational packages with aggradational topsets and thin foresets and bottomsets (blue shaded areas in Figures 3b and 9a). The aggradational topsets exhibit blocky well-log patterns of low gamma-ray responses versus high spontaneous-potential responses (e.g. W1511), whereas thin bottomsets display higher gamma-ray responses close to the shale baseline (e.g. W3412 and W3524) (Figure 9). This HST architecture suggests the storage of large volumes of sediments on the inner shelf (i.e. inner-shelf deltas), with little or no delivery of coarse detritus into deepwater to form fans (e.g. Xu et al., 2020). This scenario of sediment-volume partitioning across the Pearl River topset is consistent with the DionisosFlow experiments during the slow sea-level rise (i.e. deltas lacking downdip fans) (Figures 5a, 7a, and 8a). High sea level and a paleo-Pearl River delta that did not reach the outer shelf most likely prohibit deep-water sand delivery, leading to no delivery of terrestrial sands into deepwater areas.

6.2 | Pearl River margin early falling-stage system tract: Deltas lack downdip fans

Seismic-well ties verify that basal and upper bounding surfaces of early falling-stage systems tract, respectively, correspond to

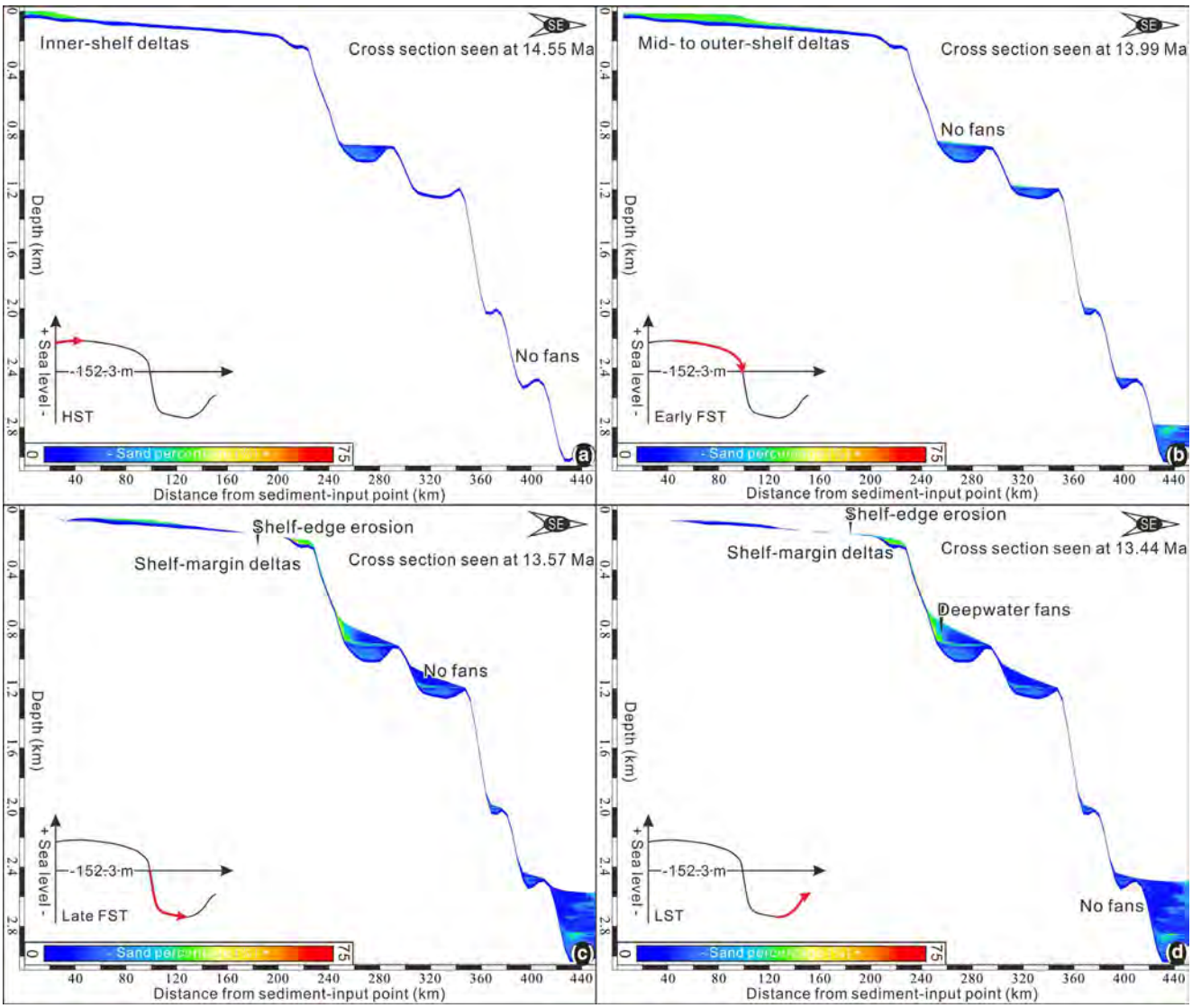

FIGURE 8 Dip-view sections of DionisosFlow forward numerical models (see their plan-view and stratigraphic locations in Figures 2 and 4, respectively) illustrating patterns of grain-size distribution at 14.55 Ma (a), 13.90 Ma (b), 13.57 Ma (c) and 13.44 Ma (d). Note that deltas seen in cross sections of panels A, B and C of this figure lack downdip fans, but that fans seen in cross sections of panel D of this figure are linked updip to significant shelf-margin erosion

the BSFR of SQ14.8 (14.4 Ma) and the within-systems tract surface (sensu Catuneanu, 2020) of SQ14.8 (i.e. WSTS of SQ14.8) (13.9 Ma) (Figures 3, 4, and 9). Clinothems bounded at their bases by the BSFR of SQ14.8 and at their tops by the WSTS of SQ14.8 exhibit an overall flattish to slightly falling shelf-edge trajectory (represented by the trajectory angle of −0.01°). They exhibit erosion at their topsets, and record a change in stacking pattern from AP stacking to dominantly progradational (Figures 3b and 9a). The prograding clinothems which occur immediately above the BSFR suggests that they can be interpreted as early falling-stage systems tract (early FST) (sensu Catuneanu, 2020) (Figures 3 and 9).

Architecturally, the Pearl River early FST of 14.4–13.9 Ma age consists of offlapping clinothems composed of flattish to slightly degrading topsets, progradational deepwater-slope foresets, and a lack of seismically recognizable aggradational bottomsets (yellow shaded areas in Figures 3b and 9a). The progradational topsets display a blocky well-log pattern consisting of low gamma-ray responses, (e.g. W3411 and W3524) (Figure 9b). Such architectural properties of early FST (especially the lack of bottomsets) suggest the storage of coarse clastics into topset and upper-slope areas, with little or no coarse detritus being partitioned into deepwater areas. This scenario of sediment-budget partitioning cross the Pearl River shelf can be compatible with DionisosFlow experiments of the slow sea-level fall (i.e. deltas lacking downdip fans) (Figures 7b, and 8b).

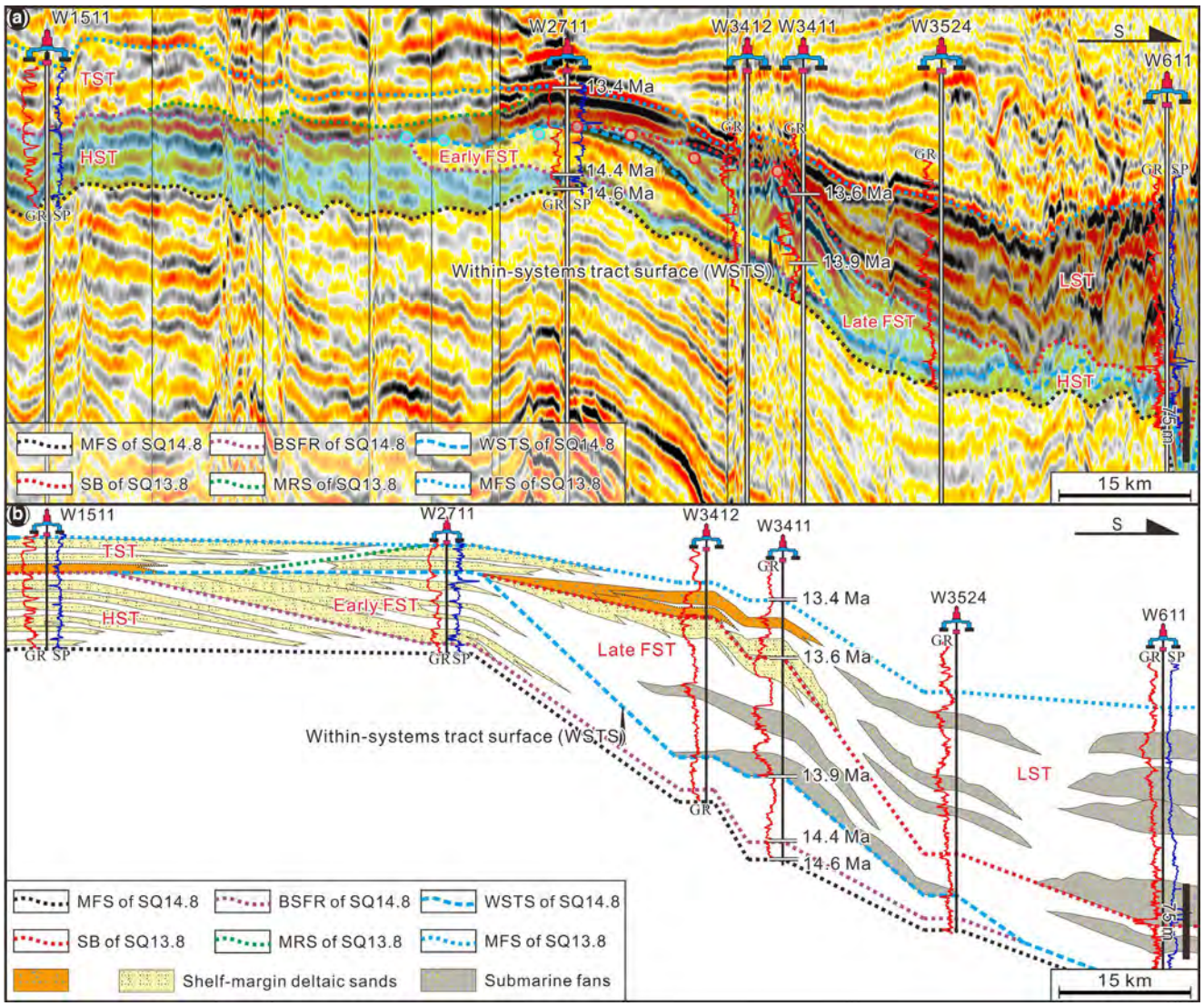

FIGURE 9 (a) Seismic-well tie transect showing architectural properties, stacking patterns, and sequence stratigraphic frameworks of 14.6–13.4 Ma Pearl River accretionary prisms. Please refer to Figures 5–8 and 10 for their corresponding DionisosFlow forward numerical models. Green and red dots in upper panel of this figure refer to flat to slightly falling and moderately falling shelf-edge trajectories, respectively. (b) Well-log, facies, stratigraphic correlation along the depositional dip showing sequence stratigraphic architectures and depositional facies of 14.6–13.4 Ma Pearl River accretionary prisms. Note that within-systems tract surface denotes the onset of submarine fan deposition

6.3 | Pearl River margin late falling-stage systems tract: Deltas linked downdip to fans

Seismic-well ties verify that the basal and upper bounding surfaces of the modeled interval of rapid sea-level fall correspond, respectively, to the within-systems-tract surface (WSTS) of SQ14.8 (13.9 Ma) and the sequence boundary of SQ13.8 (dated at 13.6 Ma) (Figures 3, 4 and 9). The interval of WSTS of SQ14.8 to SB of SQ13.8, respectively, signifies the onset of rapid sea-level fall and the end of sea-level fall (Figure 4). Clinothems in this interval exhibit an overall moderately falling shelf-edge trajectory (represented by the trajectory angle of −0.11°). They show erosion at their topsets, and record a change in stacking patterns from the dominant progradation to dominant degradation (Figures 3b and 9a). The downstepping stacking pattern of 13.9–13.6 Ma clinothems suggests that they can be considered as the late falling-stage systems tract (late FST) (Catuneanu, 2020) (Figures 3 and 9).

Architecturally, Pearl River late FST (13.9–13.6 Ma) consists of offlapping clinothems with thick, progradational foresets, thick aggradational bottomsets, but a lack of aggradational topsets (blue shaded areas in Figures 3b and 9a). The highly aggradational foresets and bottomsets of Pearl River late FST display funnel-shaped well-log patterns (being typical of deep-water fans) and contain stacked sandstones of up to 50 m thick (e.g. W3412 and W3411) (Figure 9b). Such architectural characteristics of late FST (i.e. toplap terminations

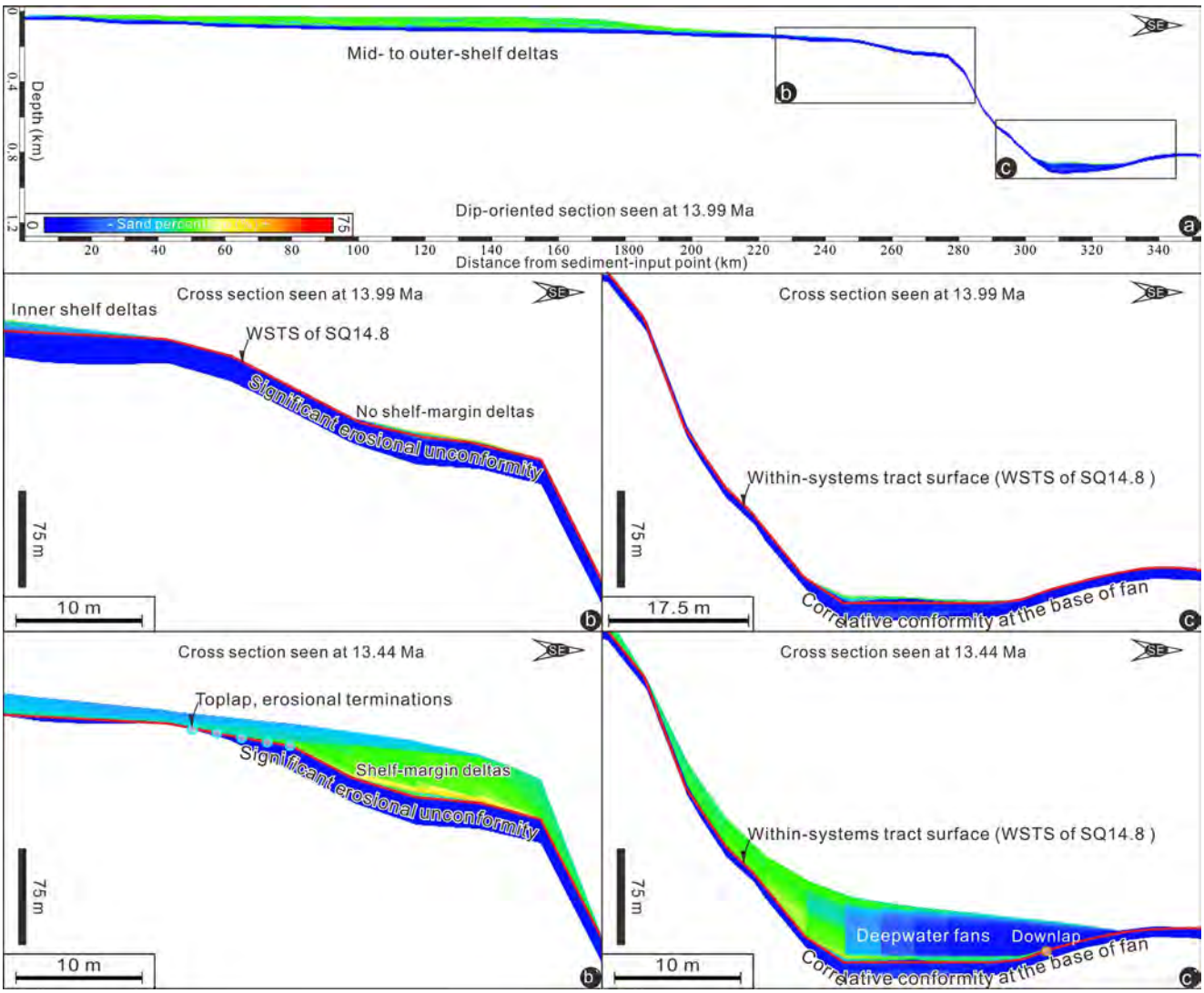

FIGURE 10 Representative cross sections of DionisosFlow forward numerical models (see Figure 2 for their map-view location) illustrating the formation of within-system tract surfaces. Within-system tract surfaces separate underlying deep-marine mudstones from overlying submarine fans. Note that within-system tract surfaces are identified as erosional unconformities at their proximal reaches, but as correlative conformities at their distal reaches

versus thick, aggradational bottomsets) indicate significant topset erosion or collapse and the resultant delivery of large volumes of terrestrial sands into the outlying deep-water, forming extensive submarine fans (Figure 10). The inferred shelf-edge erosion and the development of prominent fans are also observed in the DionisosFlow forward model of slow sea-level fall, verifying the linkages of deltas linked downdip to fans (Figure 7c).

The above linkage of shelf-margin deltas linked downdip to fans is also consolidated by observations from RMS amplitude attributes (Figure 11), on which two types of delta-to-fan S2S coupling (i.e. deltas linked downdip to fans or deltas lacking downdip fans) are seen. There are at least three main geological conditions forming the linkage between deltas and submarine fans (Figure 11). The first is a river-dominated shelf-edge delta regime, which is evidenced by the presence of shelf valleys in our DionisosFlow forward models of rapid sea-level fall (Figures 6a and 7c) and moderate sea-level rise (Figures 6b and 7d). The second is the rapid progradation of paleo-Pearl River deltas across the shelf, which would have facilitated and maintained a direct shelf-margin delta to channel connection (Figure 11). The third condition would be to have Pearl River feeder channels eating their way back to the prodelta reaches of lowstand deltas, in front of which small deep-water fans are imaged as moderate to high RMS lobes (Figure 11). Previous studies also highlighted the importance of shoreline to shelf-edge proximity in the delivery of fluvial-deltaic sediments to deepwater (Gong et al., 2019; Pellegrini et al., 2018; Sweet et al., 2020).

In marked contract to scenarios of HST and early FFST, the physical linkage of deltas lacking downdip fans as observed in Figures 11 and 12 can be ascribed to low sediment

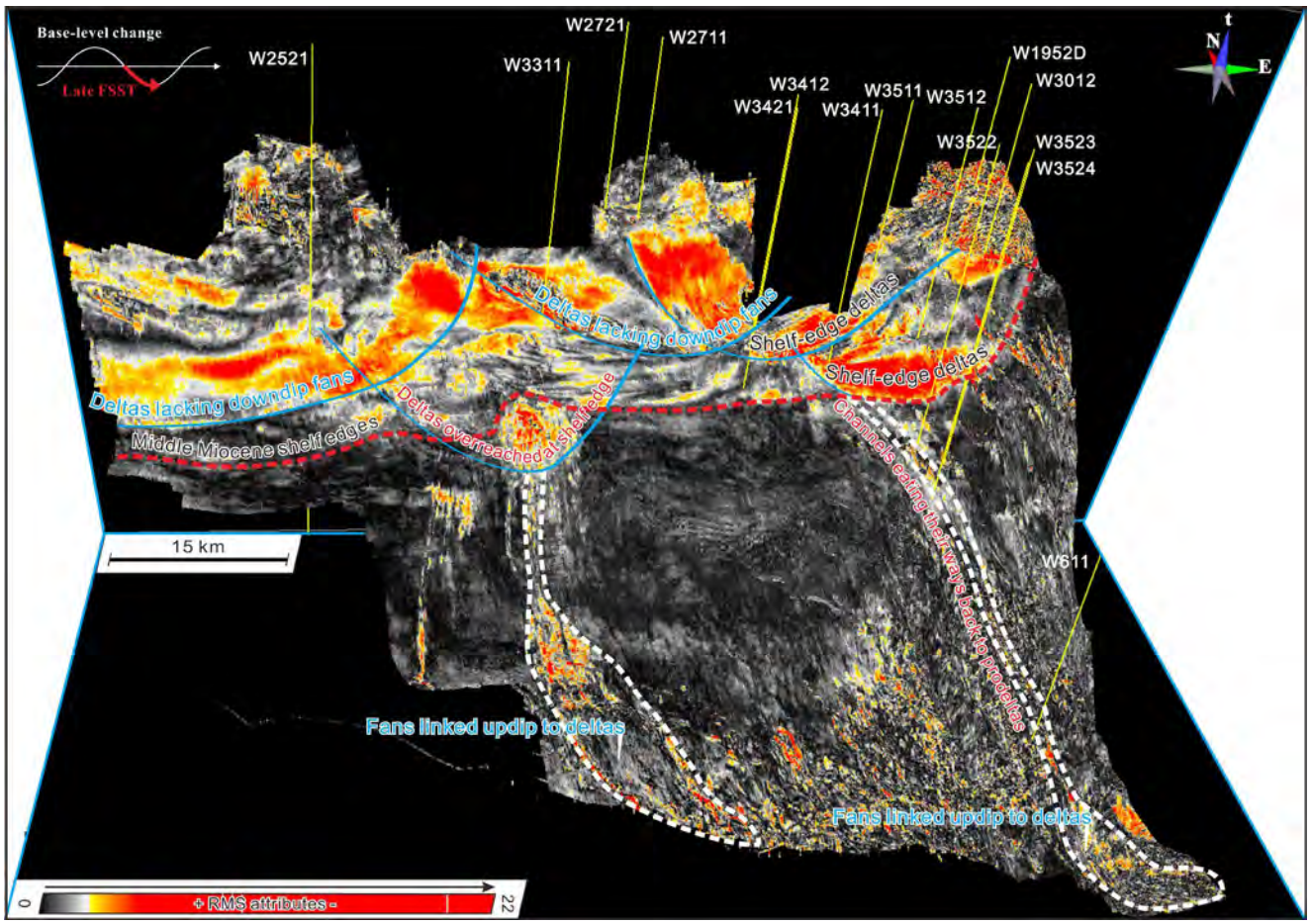

FIGURE 11 3D perspective view of RMS attributes deciphering the distribution patterns and genetic stratigraphic linkages of depositional facies developed during the deposition of late FST. The shown RMS attribute map cover the full 3D seismic survey marked by white box in Figure 2. Note that the occurrence of two types of delta-to-fan S2S coupling (i.e. deltas lacking downdip fans and fans linked updip to deltas)

supply rather than high sea levels. The western parts of Figures 11 and 12 are away from the main fairway of the middle Mocene Pearl River sediment-routing system that is located in the central and eastern parts of the utilized 3D seismic survey. They are, therefore, characterized by a low sediment supply system that was unable to push the paleo-Pearl River deltas to reside close to the shelf edge, inhibiting the delivery of deltaic sands to deep-water areas. Such deltas sited on the outer shelf (i.e. near W2512 borehole) are imaged as high RMS tongues, in front of which there are only extensive low RMS accumulations (i.e. mud-dominated slope environments) (Figures 11 and 12).

6.4 | Pearl River margin lowstand system tract: Deltas linked downdip to fans or fans lacking updip deltas

Seismic-well ties verify that basal and upper bounding surfaces of the modeled interval of modest sea-level rise correspond to the SB of SQ13.8 (13.6 Ma) and the MSF of SQ13.8 (13.4 Ma), respectively (Figures 3, 4 and 9). Clinothems within the above interval consist of sigmoidal progradational packages that contain very thin topsets and thick, highly aggradational bottomsets (blue shaded areas in Figure 3). They exhibits an overall progradation to aggradation stacking (PA stacking) (sensu Neal & Abreu, 2009), which is suggestive of rates of coastal accommodation creation and sedimentation fill ($\delta A/\delta S$) < 1 (i.e. lowstand systems tract (LST)) (e.g. Catuneanu et al., 2009; Neal & Abreu, 2009; Posamentier et al., 1992; Posamentier & Vail, 1988) (Figure 3).

Architecturally, the Pearl River LST is composed of sigmoidal progradational clinoforms with thin topsets, medium-thick deepwater-slope deposits and strongly aggradational bottomsets (blue shaded areas in Figures 3b and 9a). The bottomsets of Pearl River LST exhibit blocky to funnel-shaped well-log patterns, thereby showing an overall massive to coarsening-upward grain-size profile (being typical of submarine fans with massive sandy turbidites) (e.g. W3524 and W611) (Figure 9b). Such LST architecture suggests the continued efficient topset sediment bypass and a resultant delivery of great volumes of terrestrial sands into deepwater to

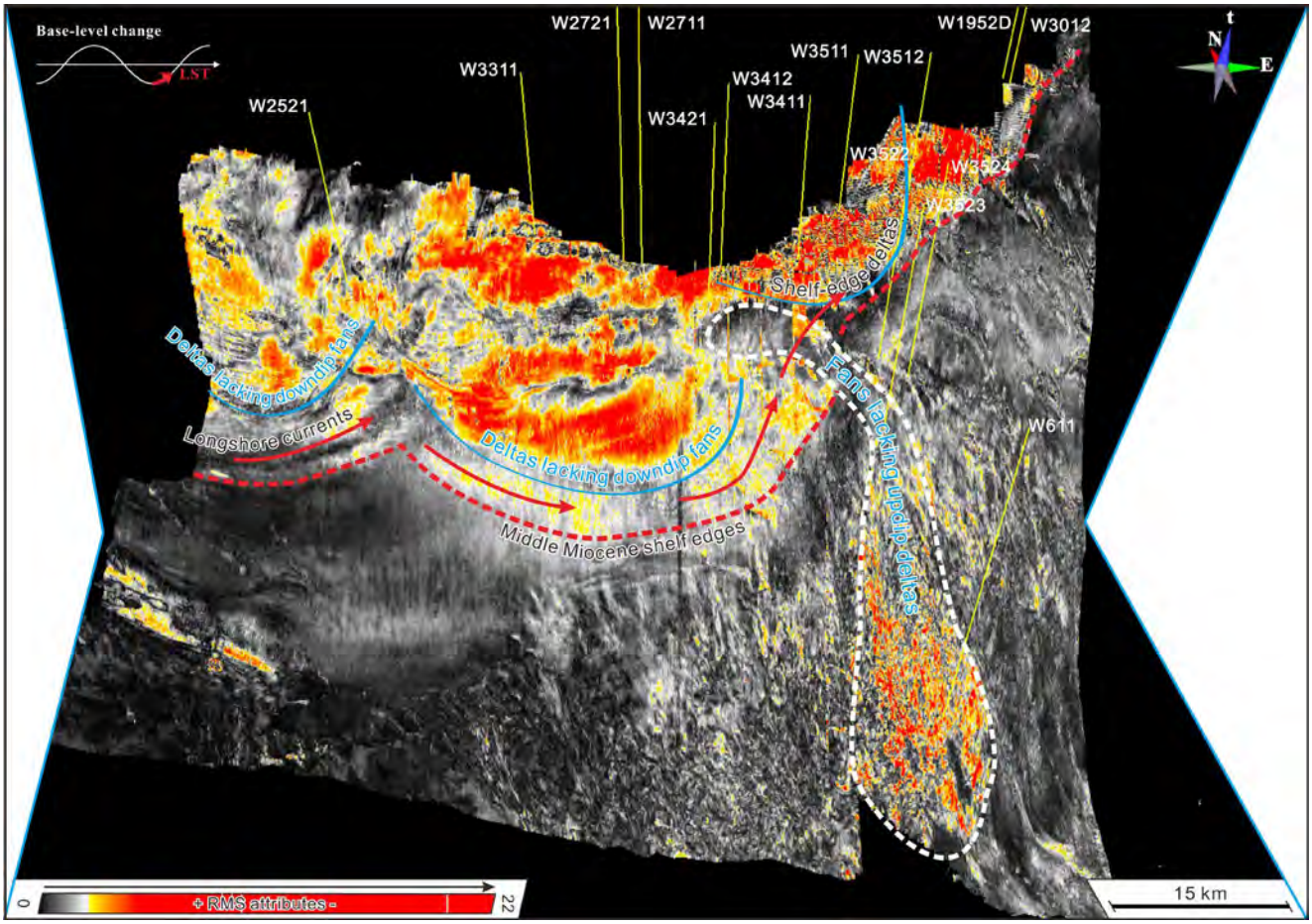

FIGURE 12 3D perspective view of RMS attributes illustrating the distribution patterns and genetic stratigraphic linkages of depositional facies developed during the deposition of LST. The shown RMS attribute map cover the full 3D seismic survey marked by white box in Figure 2. Note that the occurrence of two types of delta-to-fan S2S coupling (i.e. deltas lacking downdip fans and fans lacking updip deltas). The shelf-edge-parallel distribution pattern of prodeltaic sandstones seen in this figure indicates the influence of longshore or other shelf currents

form submarine fans (Figures 7d, 8d and 10c′). The inferred shelf-edge sediment bypass and erosion were also observed in our DionisosFlow forward model of modest sea-level rise (i.e. deltas linked downdip to fans or fans lacking updip deltas) (Figures 7d, 8d, and 10c′).

The above model of sediment dispersal across the Pearl River shelf break is consistent with observations from the RMS attribute map shown in Figure 12, in which clear delta-to-fan S2S linkages occur. Such delivery linkage is shown as extensive fans (imaged as high RMS tongues), but with apparently no deltas updip (Figure 12). This scenario of fans lacking updip deltas as observed from seismic data can possibly be ascribed to longshore or other shelf currents, as evidenced by the occurrence of shelf-margin prodeltic deposits that extend laterally in a direction parallel to the shelf edge (red arrows in Figure 12). Clastic sediments were likely laterally transported by these longshore or shelf currents, then captured by a canyon or channel and finally delivered downdip to form deep-water fans. The role of sand transported alongshore in littoral cells, eventually captured by submarine canyons is also well documented by Walsh and Nittrouer (2003) and Bernhardt et al. (2016).

7 | CONCEPTUAL IMPLICATIONS

7.1 | Delta-to-fan S2S coupling as useful predictors of sand partitioning into deepwater

The holistic S2S approach has led to a new generation of research, and has emerged with a broader focus than previous approaches (e.g. Allen, 2008; Martinsen et al., 2010; Matenco et al., 2013; Talling et al., 2015). This approach is now beginning to be used to further explore when and how terrestrial sediments delivered into a basin are partitioned by volume, by facies and by grain size between different segments of the sediment-routing system (e.g. Matenco et al., 2013; Michael et al., 2014; Sømme et al., 2009). Predictability of sand-prone and mud-prone segments of a S2S system is especially important for reservoir and source-rock occurrence and development,

although there has been a tendency to weight provenance variability and provenance mixing (Allen et al., 2013; Michael et al., 2014). However, the provenance weight in current S2S analysis is complicated by the sparse coverage in source areas (Sømme, Helland-Hansen, Martinsen, et al., 2009) and by the difficulty in interpreting provenance data as soon as the sediment volumes reach a coastline and become far traveled by the extensive longshore movement of terrestrial sediments. DionisosFlow stratigraphic-forward models, coupled to seismic and borehole data, suggest that middle Miocene Pearl River delta-to-fan S2S coupling was stratigraphically enacted in three ways: deltas lacking downdip fans, deltas linked downdip to fans, and fans lacking updip deltas. These three ways of delta-to-fan S2S coupling are schematically illustrated in Figure 13b. We propose that further S2S studies on direct-fed margins should focus more on the segments between shoreline and sink where we yet have much to learn. For example, shelf and shelf-edge delta sediment volumes can be seen as 'sources' and can be traced via canyons, slope channels, contour and bottom currents, slope collapse and mass-transport complexes to eventual terminal depositional 'sinks' (Figure 13a).

From the perspective of sequence stratigraphy, the concept of delta-to-fan S2S coupling will help refine the existing sequence stratigraphic models that suggest relative sea-level fall represents the optimum possibility of sand accumulations

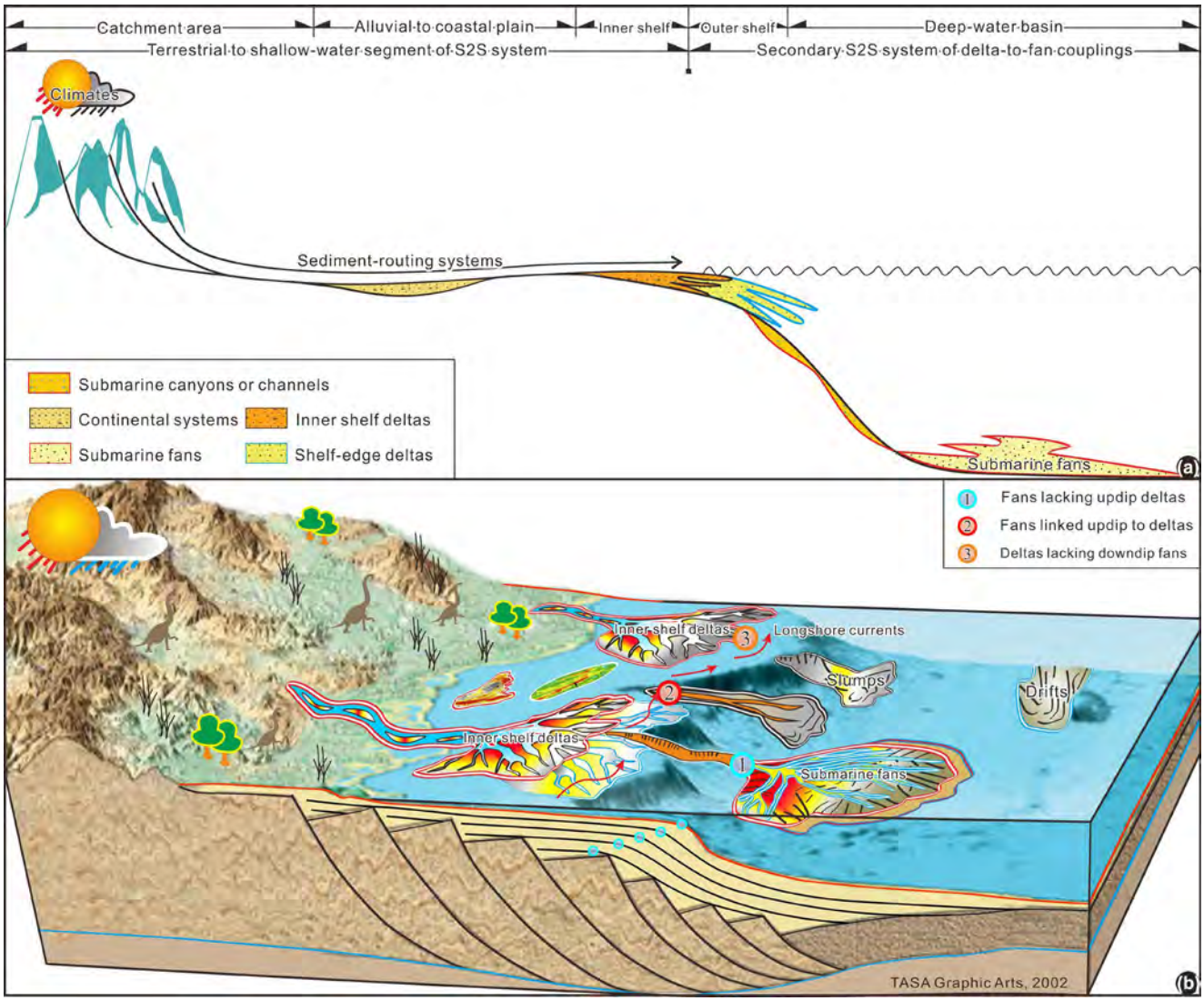

FIGURE 13 (a) Schematic portrayal of the subdivision of a land to ocean S2S system divided into a terrestrial to shallow-water segment and a submarine segment. Submarine segment of the land to ocean S2S system is composed mainly of shelf-edge deltas and resultant deep-water fans on direct-fed margins, fostering a more readily studied, secondary S2S system (i.e. delta-to-fan S2S coupling), in which shelf-edge deltas are 'sources' and deep-water fans are terminal depositional 'sinks', with canyons and/or slope channels working as delivery 'conduits' in between (Figure 1b). (b) Schematic illustration of three types of delta-to-fan S2S coupling extracted from DionisosFlow forward numerical models and 3D seismic data. Note that the existence of delta-to-fan S2S linkages guarantees the delivery of coarse detritus to deep-water areas, but that a lack of delta-to-fan S2S linkages prohibits the delivery of coarse detritus to deepwater

in deep-water areas (Catuneanu et al., 2009; Posamentier et al., 1992; Posamentier & Vail, 1988), in addition to high sediment supply (Carvajal & Steel, 2006), narrow shelves (e.g. Covault et al., 2007), and the proximity of the shoreline to a canyon head (e.g. Sweet & Blum, 2016). Our numerical simulation and seismic datasets suggest that a lack of delta-to-fan S2S linkage prohibits the delivery of coarse clastics to deep-water areas on direct-fed margins, irrespective of sea level, sediment supply, shelf width, and the proximity of shoreline to canyon heads (Figure 13b). The delta-to-fan S2S linkage is a necessary condition for the delivery of coarse detritus into submarine fans (Figure 13b). It, therefore, plays a critical but underappreciated role in delivering coarse clastics into deepwater, helping to refine the existing sequence stratigraphic models. Moreover, in along-strike direction, the documented delta-to-fan S2S linkage exhibits the significant lateral variability. More specifically, deltas linked downdip to fans, deltas lacking downdip fans and fan lacking updip deltas can coexist even within a single systems tract such as the lowstand system tract (Figure 6). Our results, therefore, represent a contribution to the on-going development of sequence stratigraphy that embraces the increasing emphasis on 3-D stratal complexity in the sense of downdip and along-strike variability (e.g. Burgess, 2016; Madof et al., 2016; Steventon et al., 2020).

From an exploration standpoint, most of the time, in terms of data, interpreters have access to a coverage going from the shelf to basin areas (e.g. 2D to 3D seismic data), without necessarily having access to the information about the 'regional' source/provenance. The concept of delta-to-fan S2S coupling, therefore, helps to improve our predictability of sand-prone and mud-prone segments of a S2S system, especially on some direct-fed margins (e.g. middle Miocene Pearl River margin). There are at least four main indicators of delta-to-fan S2S linkages, including (a) river-dominated shelf-edge regimes, (b) deltas overreach at shelf break, (c) channels extending back to prodeltas, and (d) shelf-edge-parallel distribution pattern of prodeltaic sandstones (Figures 6, 11 and 12). It should be possible in some frontier basins to identify these indicators even on coarse grids of 2D seismic data, which represents the highest possibility of sand deposition in deep-water areas, assisting greatly in predicting the occurrence of deep-water fans.

7.2 | Within-systems tract surfaces as useful predictors of extensive fan occurrence

Our DionisosFlow stratigraphic-forward models suggest the development of within-systems tract surfaces (Figures 4 and 10). We suggest that within-system tract surfaces are identified as significant lower-order, erosional unconformities at their proximal reaches and correlative conformities distally (Figures 3, 9, and 10). They are the product of a transition in sea-level behaviour from slowly falling to rapidly falling, which eroded the subaerially exposed sediment surface of earlier shelf-margin successions, and are thus diachronous (i.e. low-order sequence boundaries) (Figures 3, 4, 9, and 10). Within-system tract surfaces are characterized by: (a) a transition in trajectory regimes from flat to slight fall (represented by the trajectory angle of −0.01°) to moderate fall (represented by the trajectory angle of −0.11°) (green and red dots in Figure 9a, respectively); (b) a change in clinothem-stacking patterns from progradational-degradational staking to dominantly degradational stacking (Figures 3 and 9); (c) toplap, erosional terminations at their proximal reaches but downlap, depositional terminations at their outlying deepwater reaches (blue and orange dots in Figures 3b, 9a, and 10); and (d) the occurrence of high gamma ray "necks" immediately below them (Figure 9a,b). Although many features listed herein can be ascribed to either sequence boundaries or systems tract boundaries, the association of several of them will enhance the chance of recognizing within-systems tract surfaces.

From an exploration viewpoint, within-systems tract surfaces are boundaries that likely denote the onset of submarine fan deposition (Figures 3, 9, and 10). Recognition criteria of within-systems tract surfaces listed above can thus be a useful predictor of submarine fan occurrence, assisting greatly in predicting the occurrence of deep-water fans. Across the spectrum of existing sequence stratigraphic models, the significance of within-systems tract surfaces does not receive the same attention as other key stratigraphic surfaces (Catuneanu et al., 2009; Neal & Abreu, 2009; Posamentier & Vail, 1988). Results from the current study may help to refine the existing sequence stratigraphic models that unconsciously ignore the significance of within-systems tract surfaces. When within sequence stratigraphic surfaces are taken into account, they can highlight that sandy deposits can be compartmentalized even within a single systems tract (Pellegrini et al., 2017).

7.3 | Shelf-edge processes regimes can be vital

Our DionisosFlow stratigraphic-forward models of rapid sea-level fall and moderate sea-level rise suggest that a river-dominated shelf-edge regime is by far the most successful shelf-edge processes for getting shelfal sands to deep-water sites to form extensive fans (Figures 6a,b and 7c,d). This hypothesis is also highlighted by Dixon et al. (2012) and Paumard et al. (2020), who all suggested that the run-out distance of the turbidite systems and slope gradients increase with the importance of fluvial processes along the shelf edge. However, DionisosFlow stratigraphic-forward models

of moderate sea-level rise suggest that longshore or oceanic currents moving sediment laterally are also sometimes able to foster fans that lack updip deltas (Figures 6b and 7d). This hypothesis coincides with the scenario of fans lacking updip deltas, that can possibly be ascribed to longshore or other shelf currents, as evidenced by shelf-edge-parallel distribution pattern of prodeltaic sandstones (Figure 12). In such cases, deep-water delivery sites (i.e. submarine fans) are not necessarily downdip of shelf-edge deltas, but farther along strike because of longshore drift at the shelf edge.

8 | CONCLUSIONS

We employ a DionisosFlow stratigraphic-forward model, coupled to seismic and borehole data, to evaluate the role of delta-to-fan S2S coupling for the delivery of clastic detritus into deepwater. The significance of our work is to show in more detail how and when delta-to-fan S2S coupling can occur between deltas and submarine fans and how these linkages regulate the quantity and caliber of coarse clastics being partitioned into deepwater areas of direct-fed margins.

Stratigraphic-forward model results suggest that delta-to-fan S2S linkages are stratigraphically enacted in three ways (i.e. deltas lacking downdip fans, deltas linked downdip to fans, and fans lacking updip deltas), and that a rapid change in sea-level behaviour from slowly falling to rapidly falling produce the within-system tract surface. The within-system tract surface divides the FST into two components (i.e. early FST and late FST), and signifies the onset of submarine fan deposition, with applications to the sequence-stratigraphic predilection of submarine fan occurrence.

Seismic and borehole results suggest that: (a) deltas lacking downdip fans can be ascribed to high sea level, low sediment supply or strong storm wave influence at the shelf edge; (b) deltas linked downdip to fans may be related to river-dominated shelf-edge regimes, delta overreach at shelf break or channels extending back to prodelta areas; and that (c) fans lacking updip deltas can be ascribed to longshore or oceanic currents moving sediment laterally, though these can then be taken into a canyon and brought directly to the basin floor. Within-system tract surfaces are identified as erosional unconformities in their proximal reaches and their correlative conformities distally, and can be recognized by a change in shelf-edge trajectory from flat to slight fall to moderate fall and a change in stacking patterns from mixed progradation and degradation to dominant degradation.

ACKNOWLEDGEMENTS

This research was jointly funded by the National Natural Science Foundation of China (Nos. 41802117 and 41902114) and by the Science Foundation of China University of Petroleum, Beijing (No. 2462020YXZZ020). The authors thank the academic license of DionisosFlow provided by the Beicip-Franlab. The authors also thank BR editor (Dr. Wonsuck Kim) for editorial handing and comments and to BR reviewers (Dr. Victorien Paumard and an anonymous reviewer) for their insightful and constructive comments, all of which significantly improved the overall quality of this research.

CONFLICT OF INTEREST

No conflict of interest is declared.

PEER REVIEW

The peer review history for this article is available at https://publons.com/publon/10.1111/bre.12591.

DATA AVAILABILITY STATEMENT

The data that support the findings of this study are available from the corresponding author upon reasonable request. Restrictions apply to the availability of these data, which were used under license for this study.

REFERENCES

Allen, P. (2008). From landscapes into geological history. *Nature*, *451*, 274–276. https://doi.org/10.1038/nature06586

Allen, P. A., Armitage, J. J., Carter, A., Duller, R. A., Michael, N. A., Sinclair, H. D., Whitchurch, A. L., & Whittaker, A. C. (2013). The supply problem: Sediment volumetric balance of proximal foreland basin systems. *Sedimentology*, *60*, 102–130.

Bernhardt, A., Hebbeln, D., Regenberg, M., Lückge, A., & Strecker, M. R. (2016). Shelfal sediment transport by an undercurrent forces turbidity current activity during high sea level along the Chile continental margin. *Geology*, *44*, 295–298. https://doi.org/10.1130/G37594.1

Burgess, P. M. (2016). RESEARCH FOCUS: The future of the sequence stratigraphy paradigm: Dealing with a variable third dimension. *Geology*, *44*, 335–336. https://doi.org/10.1130/focus042016.1

Cao, L., Shao, L., Qiao, P., Zhao, Z., van Hinsbergen, D. J. J. (2018). Early Miocene birth of modern Pearl River recorded low-relief, high-elevation surface formation of SE Tibetan Plateau. *Earth and Planetary Science Letters*, *496*, 120–131. https://doi.org/10.1016/j.epsl.2018.05.039

Carvajal, C., & Steel, R. (2006). Thick turbidite successions from supply-dominated shelves during sea-level highstand. *Geology*, *34*, 665–668. https://doi.org/10.1130/G22505.1

Catuneanu, O. (2020). Sequence stratigraphy of deep-water systems. *Marine and Petroleum Geology*, *114*, 104238. https://doi.org/10.1016/j.marpetgeo.2020.104238

Catuneanu, O., Abreu, V., Bhattacharya, J. P., Blum, M. D., Dalrymple, R. W., Eriksson, P. G., Fielding, C. R., Fisher, W. L., Galloway, W. E., Gibling, M. R., Giles, K. A., Holbrook, J. M., Jordan, R., Kendall, C. G. S. C., Macurda, B., Martinsen, O. J., Miall, A. D., Neal, J. E., Nummedal, D., … Winker, C. (2009). Towards the standardization of sequence stratigraphy. *Earth-Science Reviews*, *92*, 1–33. https://doi.org/10.1016/j.earscirev.2008.10.003

Covault, J. A., Normark, W. R., Romans, B. W., & Graham, S. A. (2007). Highstand fans in the California borderland: The overlooked deepwater depositional systems. *Geology*, *35*, 783–786. https://doi.org/10.1130/G23800A.1

Covault, J. A., Romans, B. W., Fildani, A., McGann, M., & Graham, S. A. (2010). Rapid climatic signal propagation from source to sink in a southern California sediment-routing system. *The Journal of Geology*, *118*, 247–259. https://doi.org/10.1086/651539

Deville, E., Mascle, A., Callec, Y., Huyghe, P., Lallemant, S., Lerat, O., Mathieu, X., Padron de Carillo, C., Patriat, M., Pichot, T., Loubrieux, B., & Granjeon, D. (2015). Tectonics and sedimentation interactions in the east Caribbean subduction zone: An overview from the Orinoco delta and the Barbados accretionary prism. *Marine and Petroleum Geology*, *64*, 76–103. https://doi.org/10.1016/j.marpetgeo.2014.12.015

Dixon, J. F., Steel, R. J., & Olariu, C. (2012). Shelf-edge delta regime as a predictor of the deep-water deposition. *Journal of Sedimentary Research*, *82*, 681–687.

Fisher, W. L., Galloway, W. E., Steel, R. J., Olariu, C., Kerans, C., & Mohrig, D. (2021). Deep-water depositional systems supplied by shelf-incising submarine canyons: Recognition and significance in the geologic record. *Earth-Science Reviews*, *214*, 103531. https://doi.org/10.1016/j.earscirev.2021.103531

Gong, C., Blum, M. D., Wang, Y., Lin, C., & Qiang, X. (2018). Can climatic signals be discerned in the deepwater sink? An answer from the Pearl River sediment-routing system. *GSA Bulletin*, *130*, 661–677.

Gong, C., Qi, K., Ma, Y., Li, D., Feng, N., & Xu, H. (2019). Tight coupling between the cyclicity of deep-water systems and rising-then-flat shelf-edge pairs along the submarine segment of the Qiongdongnan sediment routing system. *Journal of Sedimentary Research*, *89*, 956–975. https://doi.org/10.2110/jsr.2019.47

Gong, C., Steel, R. J., Wang, Y., Lin, C., & Olariu, C. (2016). Grain size and transport regime at shelf edge as fundamental controls on delivery of shelf-edge sands to deepwater. *Earth-Science Reviews*, *154*, 72–101.

Granjeon, D. (2014). 3D forward modelling of the impact of sediment transport and base level cycles on continental margins and incised valleys. In A. W. Martinius, R. Ravnås, J. A. Howell, R. J. Steel & J. P. Wonham (Eds.), *From depositional systems to sedimentary successions on the Norwegian continental margin* (1st ed., Vol. *46*, pp. 453–472). Int. Assoc. Sedimentol. Spec. Publ.

Harris, A. D., Baumgardner, S. E., Sun, T., & Granjeon, D. (2018). A poor relationship between sea level and deep-water sand delivery. *Sedimentary Geology*, *370*, 42–51. https://doi.org/10.1016/j.sedgeo.2018.04.002

Harris, A. D., Covault, J. A., Baumgardner, S. E., Sun, T., & Granjeon, D. (2020). Numerical modeling of icehouse and greenhouse sea-level changes on a continental margin: Sea-level modulation of deltaic avulsion processes. *Marine and Petroleum Geology*, *111*, 807–814. https://doi.org/10.1016/j.marpetgeo.2019.08.055

Harris, A. D., Covault, J. A., Madof, A. S., Sun, T., Sylvester, Z., & Granjeon, D. (2016). Three-dimensional numerical modeling of eustatic control on continental-margin sand distribution. *Journal of Sedimentary Research*, *86*, 1434–1443. https://doi.org/10.2110/jsr.2016.85

Hawie, N., Covault, J. A., Dunlap, D., & Sylvester, Z. (2018). Slope-fan depositional architecture from high-resolution forward stratigraphic models. *Marine and Petroleum Geology*, *91*, 576–585. https://doi.org/10.1016/j.marpetgeo.2017.12.033

Hawie, N., Covault, J. A., & Sylvester, Z. (2019). Grain-size and discharge controls on submarine fan depositional patterns from forward stratigraphic models. *Frontiers in Earth Science*, *7*, 334. https://doi.org/10.3389/feart.2019.00334

Holbourn, A., Kuhnt, W., Lyle, M., Schneider, L., Romero, O., & Andersen, N. (2014). Middle Miocene climate cooling linked to intensification of eastern equatorial pacific upwelling. *Geology*, *42*, 19–22. https://doi.org/10.1130/G34890.1

Hunt, D., & Tucker, M. E. (1992). Stranded parasequences and the forced regressive wedge systems tract: Deposition during base-level fall. *Sedimentary Geology*, *81*, 1–9. https://doi.org/10.1016/0037-0738(92)90052-S

Jones, G. E. D., Hodgson, D. M., & Flint, S. S. (2014). Lateral variability in clinoform trajectory, process regime, and sediment dispersal patterns beyond the shelf-edge rollover in exhumed basin margin-scale clinothems. *Basin Research*, *27*, 657–680. https://doi.org/10.1111/bre.12092

Kim, Y., Kim, W., Cheong, D., Muto, T., & Pyles, D. (2013). Piping coarse-grained sediment to a deep-water fan through a shelf-edge delta bypass channel: Tank Experiments. *Journal of Geophysical Research – Earth Surface*, *118*, 2279–2291. https://doi.org/10.1002/2013JF002813

Koo, W., Olariu, C., Steel, R. J., Olariu, M. I., Carvajal, C. R., & Kim, W. (2016). Coupling between shelf-edge architecture and submarine-fan growth style in a supply-dominated margin. *Journal of Sedimentary Research*, *86*, 613–628. https://doi.org/10.2110/jsr.2016.42

Li, C. F., Li, J. B., Ding, W. W., Franke, D., Yao, Y. J., Shi, H. S., Pang, X., Cao, Y., Lin, J., Kulhanek, D. K., Williams, T., Bao, R., Briais, A., Brown, E. A., Chen, Y., Clift, P. D., Colwell, F. S., Dadd, K. A., Hernández-Almeida, I., … Zhao, X. (2015). Seismic stratigraphy of the central South China Sea basin and implications for neotectonics. *Journal of Geophysical Research-Solid Earth*, *120*, 1–23. https://doi.org/10.1002/2014JB011686

Lin, C., He, M., Steel, R. J., Zhang, Z., Lia, H., Zhang, B., Wu, W., Shu, L., Tian, H., Zhang, X., Xing, Z., Wang, S., & Zhang, M. (2018). Changes in inner- to outer-shelf delta architecture, Oligocene to Quaternary Pearl River shelf-margin prism, northern South China Sea. *Marine Geology*, *404*, 187–204. https://doi.org/10.1016/j.margeo.2018.07.009

Lin, C., Jiang, J., Shi, H., Zhang, Z., Liu, J., Qin, C., Li, H., Ran, H., Wei, A., Tian, H., Xing, Z., & Yao, Q. (2018). Sequence architecture and depositional evolution of the northern continental slope of the South China Sea: Responses to tectonic processes and changes in sea level. *Basin Research*, *30*, 568–595. https://doi.org/10.1111/bre.12238

Madof, A. S., Harris, A. D., & Connell, S. D. (2016). Nearshore along-strike variability: Is the concept of the systems tract unhinged? *Geology*, *44*, 315–318. https://doi.org/10.1130/G37613.1

Martin, J., Paola, C., Abreu, V., Neal, J., & Sheets, B. (2009). Sequence stratigraphy of experimental strata under known conditions of differential subsidence and variable base level. *AAPG Bulletin*, *93*, 503–533. https://doi.org/10.1306/12110808057

Martinsen, O. J., Sømme, T. O., Thurmond, J. B., Helland-Hansen, W., & Lunt, I. (2010). Source-to-sink systems on passive margins: theory and practice with an example from the Norwegian continental margin. In B. A. Vining & S. C. Pickering (Eds.), *From mature basins to new frontiers – Proceedings of the 7th petroleum geology conference* (Vol. *7*, pp. 913–920). Geological Society.

Matenco, L., Andriessen, P.; the Source Sink Network. (2013). Quantifying the mass transfer from mountain ranges to deposition in sedimentary basins: Source to sink studies in the Danube basin-Black Sea system. *Global and Planetary Change*, *103*, 1–18. https://doi.org/10.1016/j.gloplacha.2013.01.003

Mellere, D., Breda, A., & Steel, R. J. (2003). Fluvially incised shelf-edge deltas and linkage to upper-slope channels (Central Tertiary Basin in Spitsbergen). In H. H. Roberts, N. C. Rosen, R. H. Fillon, & J. B. Anderson (Eds.), *Shelf margin deltas and linked down slope petroleum systems (CD-ROM)* (Vol. *23*, pp. 231–266). SEPM Special Publication.

Michael, N. A., Whittaker, A. C., Carter, A., & Allen, P. A. (2014). Volumetric budget and grain-size fractionation of a geological sediment routing system: Eocene Escanilla Formation, south-central Pyrenees. *GSA Bulletin*, *126*, 585–599. https://doi.org/10.1130/B30954.1

Milliman, J. D., & Syvitski, J. P. (1992). Geomorphic/tectonic control of sediment discharge to the ocean: The importance of small mountainous rivers. *The Journal of Geology*, *100*, 525–544. https://doi.org/10.1086/629606

Mitchum, R. M. Jr., & Van Wagoner, J. C. (1991). High-frequency sequences and their stacking patterns; sequence-stratigraphic evidence of high-frequency eustatic cycles. In K. T. Biddle & W. Schlager (Eds.), *The record of sea-level fluctuations*. Sedimentary Geology (Vol. *70*, pp. 131–160).

Neal, J., & Abreu, V. (2009). Sequence stratigraphy hierarchy and the accommodation succession method. *Geology*, *37*, 779–782. https://doi.org/10.1130/G25722A.1

Paumard, V., Bourget, J., Payenberg, T., George, A. D., Ainsworth, R. B., & Lang, S. (2019). From quantitative 3D seismic stratigraphy to sequence stratigraphy: Insights into the vertical and lateral variability of shelf-margin depositional systems at different stratigraphic orders. *Marine and Petroleum Geology*, *110*, 797–831. https://doi.org/10.1016/j.marpetgeo.2019.07.007

Paumard, V., Bourget, J., Payenberg, T., George, A. D., Ainsworth, R. B., Lang, S., & Posamentier, H. W. (2020). Controls on deep-water sand delivery beyond the shelf edge: Accommodation, sediment supply, and deltaic process regime. *Journal of Sedimentary Research*, *90*, 104–130. https://doi.org/10.2110/jsr.2020.2

Pellegrini, C., Asioli, A., Bohacs, K. M., Drexler, T. M., Feldman, H. R., Sweet, M. L., Maselli, V., Rovere, M., Gamberi, F., Valle, G. D., & Trincardi, F. (2018). The late Pleistocene Po River lowstand wedge in the Adriatic Sea: Controls on architecture variability and sediment partitioning. *Marine and Petroleum Geology*, *96*, 16–50. https://doi.org/10.1016/j.marpetgeo.2018.03.002

Pellegrini, C., Maselli, V., Gamberi, F., Asioli, A., Bohacs, K. M., Drexler, T. M., & Trincardi, F. (2017). How to make a 350-m-thick lowstand systems tract in 17,000 years: The Late Pleistocene Po River (Italy) lowstand wedge. *Geology*, *45*, 327–330. https://doi.org/10.1130/G38848.1

Pellegrini, C., Patruno, S., Helland-Hansen, W., Steel, R. J., & Trincardi, F. (2020). Clinoforms and clinothems: Fundamental elements of basin infill. *Basin Research*, *32*, 187–205. https://doi.org/10.1111/bre.12446

Peng, Y., Steel, R. J., & Olariu, C. (2017). Transition from storm wave-dominated outer shelf to gullied upper slope: The mid-Pliocene Orinoco shelf margin, South Trinidad. *Sedimentology*, *64*, 1511–1539. https://doi.org/10.1111/sed.12362

Posamentier, H. W., Allen, G. P., James, D. P., & Tesson, M. (1992). Forced regressions in a sequence stratigraphic framework: Concepts, examples, and exploration significance. *AAPG Bulletin*, *76*, 1687–1709.

Posamentier, H. W., Jervey, M. T., & Vail, P. R. (1988). Eustatic controls on clastic deposition II — sequence and systems tract models. In C. K. Wilgus, B. S. Hastings, C. G. S. C. Kendall, H. W. Posamentier, C. A. Ross, & J. C. van Wagoner (Eds.), *Sea-level change: An integrated approach* (Vol. *42*, pp. 109–124). SEPM Special Publications.

Posamentier, H. W., & Vail, P. R. (1988). Eustatic controls on clastic deposition II–Sequence and systems tract models. In C. K. Wilgus, B. S. Hastings, H. W. Posamentier, J. Van Wagoner, C. A. Ross, & G. G. S. C. Kendall (Eds.), *Sea-level changes: An integrated approach* (Vol. *42*, pp. 125–154). SEPM Special Publication.

Prosser, I. P., & Rustomji, P. (2000). Sediment transport capacity relations for overland flow. *Progress in Physical Geography*, *24*(2), 179–193.

Ran, H., Lin, C., Dai, Y., Qin, C., Wu, W., Zhang, Y., & Qiao, Y. (2013). Sedimentary sequence and lithologic-stratigraphic trap of the middle segment of Hanjiang formation in the shelf break zone in southeast Panyu natural gas areal, Pearl River Mouth Basin [in Chinese]. *Acta Sedimentologica Sinica*, *31*, 1081–1019.

Shao, L., Pang, X., Qiao, P., Chen, C., Li, Q., & Miao, W. (2008). Sedimentary filling of the Pear River Mouth Basin and its response to the evolution of the Pearl River [in Chinese]. *Acta Sedimentologica Sinica*, *26*, 179–185.

Sømme, T. O., Helland-Hansen, W., & Granjeon, D. (2009). Impact of eustatic amplitude variations on shelf morphology, sediment dispersal, and sequence stratigraphic interpretation: Icehouse versus greenhouse systems. *Geology*, *37*, 587–590. https://doi.org/10.1130/G25511A.1

Sømme, T. O., Helland-Hansen, W., Martinsen, O. J., & Thurmond, J. (2009). Relationships between morphological and sedimentological parameters in source-to-sink systems: A basis for predicting semi-quantitative characteristics in subsurface systems. *Basin Research*, *21*, 361–387. https://doi.org/10.1111/j.1365-2117.2009.00397.x

Steel, R. J., Plink-Bjorklund, P., Porębski, S. J., Mellere, D., & Schellpeper, M. (2003). Shelf-edge delta types and their sequence-stratigraphic relationships. In H. Roberts, N. Rose, R. H. Fillon, & J. B. Anderson (Eds.), *Shelf margin deltas and linked down slope petroleum systems* (Vol. *23*, pp. 205–230). SEPM Foundation.

Steventon, M. J., Jackson, C.-A.-L., Hodgson, D. M., & Johnson, H. D. (2020). Lateral variability of shelf-edge and basin-floor deposits, Santos Basin, offshore Brazil. *Journal of Sedimentary Research*, *90*, 1198–1221. https://doi.org/10.2110/jsr.2020.14

Sweet, M. L., & Blum, M. D. (2016). Connections between fluvial to shallow marine environments and submarine canyons: Implications for sediment transfer to deep water. *Journal of Sedimentary Research*, *86*, 1147–1162. https://doi.org/10.2110/jsr.2016.64

Sweet, M. L., Gaillot, G. T., Jouet, G., Rittenour, T. M., Toucanne, S., Marsset, T., & Blum, M. D. (2020). Sediment routing from shelf to basin floor in the Quaternary Golo System of Eastern Corsica, France, western Mediterranean Sea. *GSA Bulletin*, *132*, 1217–1234. https://doi.org/10.1130/B35181.1

Talling, P. J., Allin, J., Armitage, D. A., Arnott, R. W., Cartigny, M. J. B., Clare, M. A., Felletti, F., Covault, J. A., Girardclos, S., Hansen, E., Hill, P. R., Hiscott, R. N., Hogg, A. J., Hughes Clarke, J., Jobe, Z. R., Malgesini, G., Mozzato, A., Naruse, H., Parkinson, S., … Xu, J. (2015). Key future directions for research on turbidity currents and their deposits. *Journal of Sedimentary Research*, *85*, 153–169. https://doi.org/10.2110/jsr.2015.03

Tucker, G. E., & Slingerland, R. L. (1994). Erosional dynamics, flexural isostasy, and long-lived escarpments: A numerical modeling study. *Journal of Geophysical Researh. Solid Earth*, *99*, 12229–12243.

Uroza, C. A., & Steel, R. J. (2008). A highstand shelf-margin delta system from the Eocene of West Spitsbergen, Norway.

Sedimentary Geology, *203*, 229–245. https://doi.org/10.1016/j.sedgeo.2007.12.003

Vail, P. R., Mitchum, R. M. Jr., & Thompson, S. I. I. I. (1977). Seismic stratigraphy and global changes of sea level, part 4: Global cycles of relative changes of sea level. In C. W. Payton (Ed.), *Seismic stratigraphy–Applications to hydrocarbon exploration* (Vol. *26*, pp. 83–97). AAPG Memoir.

Walsh, J., & Nittrouer, C. A. (2003). Contrasting styles of off-shelf sediment accumulation in New Guinea. *Marine Geology*, *196*, 105–125. https://doi.org/10.1016/S0025-3227(03)00069-0

Wei, X., & Wu, C. (2011). Holocene delta evolution and sequence stratigraphy of the Pearl River Delta in South China. *Science China-Earth Sciences*, *54*, 1523–1541. https://doi.org/10.1007/s11430-011-4238-6

Xie, L., Zhang, B., Qin, C., Wang, Y., Chen, S., & Gao, P. (2009). Forced regression and normal regression deposition of basin with continental shelf slope-break: A case study on Zhujiang and Hanjiang Formations of Pearl River Mouth Basin [in Chinese]. *Acta Sedimentologica Sinica*, *27*, 1093–1100.

Xu, S., Han, J., Wang, Y., He, M., Pang, X., Chen, W., Gong, C., Qin, C., Li, X., & Xu, S. (2020). How much systems-tract scale, three-dimensional stratigraphic variability is present in sequence stratigraphy? An answer from the middle Miocene Pearl River Mouth Basin. *AAPG Bulletin*, *104*, 1261–1285. https://doi.org/10.1306/01222001607417001

Xu, S., Yang, S., & Huang, L. (1995). The application of sequence stratigraphy to stratigraphic correlation [in Chinese]. *Earth Science Frontier*, *2*, 115–123.

Zhang, J., Burgess, P. M., Granjeon, D., & Steel, R. (2019). Can sediment supply variations create sequences? Insights from stratigraphic forward modelling. *Basin Research*, *31*, 274–289. https://doi.org/10.1111/bre.12320

Zhang, J., Kim, W., Olariu, C., & Steel, R. (2019). Accommodation- vs. supply-dominated systems for sediment partitioning to deep water. *Geology*, *47*, 419–422.

Zhang, J., Steel, R., & Olariu, C. (2017). What conditions are required for deltas to reach the shelf edge during rising sea level? *Geology*, *45*, 1107–1110. https://doi.org/10.1130/G39676.1

Zhang, M., Lin, C., He, M., Zhang, Z., Li, H., Feng, X., Tian, H., & Liu, H. (2019). Stratigraphic architecture, shelf-edge delta and constraints on the development of the Late Oligocene to Early Miocene continental margin prism, the Pearl River Mouth Basin, northern South China Sea. *Marine Geology*, *416*, 105982. https://doi.org/10.1016/j.margeo.2019.105982

SUPPORTING INFORMATION

Additional Supporting Information may be found online in the Supporting Information section.

How to cite this article: Gong, C., Li, D., Steel, R. J., Peng, Y., Xu, S., & Wang, Y. (2021). Delta-to-fan source-to-sink coupling as a fundamental control on the delivery of coarse clastics to deepwater: Insights from stratigraphic forward modelling. *Basin Research*, 33, 2960–2983. https://doi.org/10.1111/bre.12591